Contributions to Mineralogy and Petrology (2024) 179:90
https://doi.org/10.1007/s00410-024-02172-7

ORIGINAL PAPER

Petrogenesis of the Deccan high-Mg basalts and picrites

Nilanjan Chatterjee[1]

Received: 6 June 2024 / Accepted: 11 September 2024

Abstract
Tholeiitic basalts and picrites from the Deccan Traps were used to constrain the pressure and temperature conditions of mantle melting for their origin. Clinopyroxene thermobarometry indicates that all Deccan tholeiites crystallized at low pressures in the upper crust (< 6 kbar/1047–1221 °C). In comparison, the Deccan alkalic rocks crystallized at pressures up to ~ 12.7 kbar. Rare samples of the tholeiites plot on their low-pressure olivine-plagioclase-clinopyroxene (Ol-Pl-Cpx) cotectic boundaries or olivine control lines in phase diagrams. These samples represent unmodified magmatic liquids. Primary magmas of the basalts that plot on their cotectic boundaries were modeled through reverse fractionation by incrementally adding equilibrium Ol + Pl + Cpx, Ol + Pl and Ol ± spinel, until the liquid was multiply saturated with lherzolite at a high pressure. The high-Mg basalts are contaminated with continental crust. Hence, a crustal partial melt was simultaneously subtracted according to energy constraints at each reverse fractionation step for these samples. The results show that the high-Mg basalts are 41–53% fractionated and 1–6% contaminated, and the low-Mg basalts are 63–67% fractionated. Their primary magmas were last equilibrated with spinel lherzolite at 10–13 kbar/1289–1333 °C. A picrite and two very high-Mg basalts plot on their olivine control lines. So, their primary magmas were calculated by adding only equilibrium olivine. These samples are 9–25% fractionated, and their primary magmas were last equilibrated with garnet lherzolite at 25–36 kbar/1452–1531 °C. The estimated mantle potential temperatures are 1400–1500 °C for the Deccan tholeiites, consistent with their origin from a mantle plume.

Keywords Deccan Traps · Picrite · Basalt · Tholeiite · Primary magma · Lherzolite · Crustal contamination · Reverse fractionation

Introduction

The composition of basalts provide important clues to the melting conditions of the upper mantle for their origin (Klein and Langmuir 1987; Langmuir et al. 1992; Kinzler and Grove 1992a,b; Green et al. 2001; Presnall et al. 2002; Herzberg et al. 2007; Putirka et al. 2007; Behn and Grove 2015; Krein et al. 2021; Matthews et al. 2021). Primitive high-Mg basalts and picrites are especially useful in constraining the composition of primary melts (magma) of the mantle, pressure–temperature (P–T) conditions of their origin, and potential temperature defined as the temperature of mantle if it were to adiabatically decompress and reach the Earth's surface without melting. For deep mantle plumes, the potential temperature is significantly higher than the temperature of the ambient mantle (review in Putirka et al. 2007). Primary magmas that originate by melting of lherzolite are multiply saturated (in equilibrium) with the minerals in lherzolite (e.g., olivine with ~ 90% forsterite content, ~ Fo_{90}), and they typically have an Mg# (Mg/[Mg + Fe^T] atomic ratio, where Fe^T is total Fe) of ~ 0.73 (Kinzler and Grove 1992a,b; Till et al. 2012; Grove et al. 2013; Krein et al. 2021).

Although high-Mg basalts and picrites are present among the Cretaceous-Paleogene Deccan Traps continental flood basalts of India (Fig. 1; Krishnamurthy and Cox 1977; Mahoney et al. 1985; Beane et al. 1986; Beane and Hooper 1988; Peng et al. 1994, 1998; Melluso et al. 1995; Bondre et al. 2006; Krishnamurthy et al. 2014; Cucciniello et al. 2015; Basu et al. 2020a; Sheth et al. 2022; Khanna et al. 2023), only a few studies have attempted to utilize them to estimate primary magma compositions and mantle potential

Communicated by Othmar Müntener..

✉ Nilanjan Chatterjee
nchat@mit.edu

[1] Department of Earth, Atmospheric and Planetary Sciences, Massachusetts Institute of Technology, Cambridge, MA 02139, USA

Published online: 19 September 2024

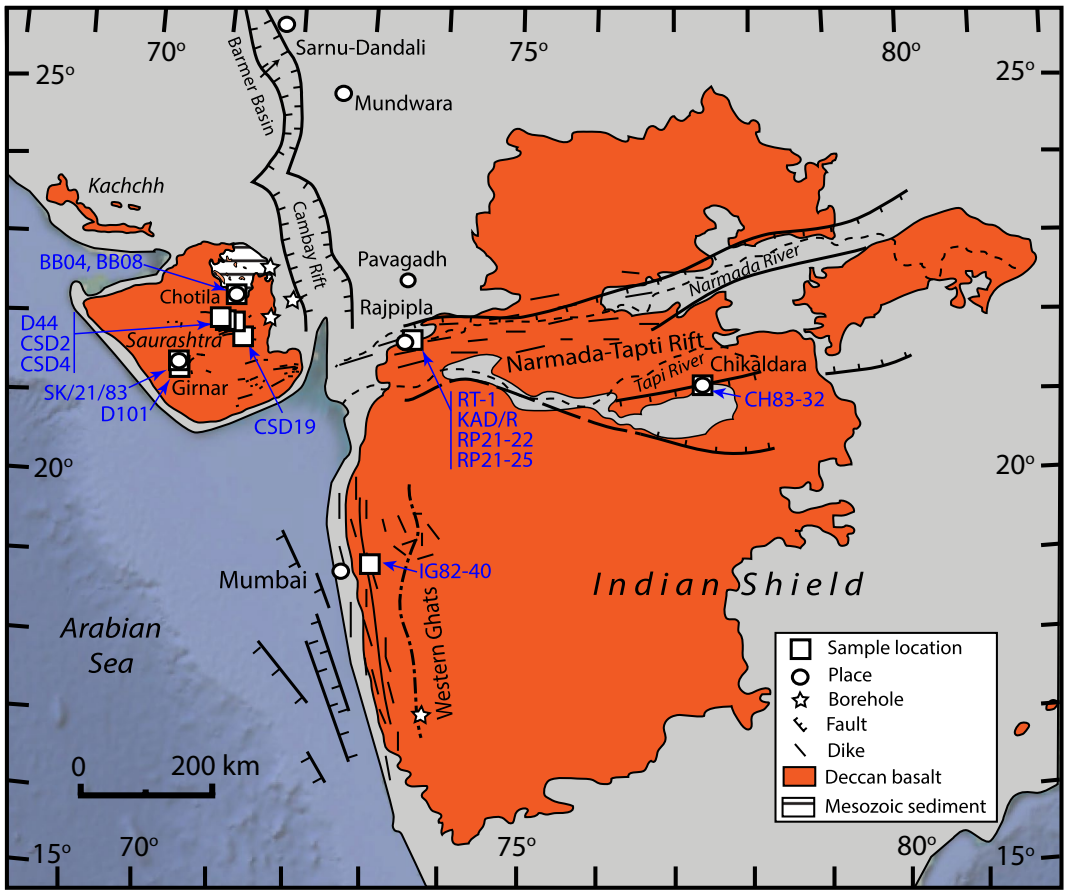

Fig. 1 Map of the Deccan Traps showing the location of samples analyzed in this study (BB04 and BB08) and samples from the literature (see text) chosen for primary magma modeling

temperatures associated with Deccan volcanism (Sen 1988, 1995; Melluso et al. 1995; Sen and Chandrasekharam 2011; Chatterjee and Sheth 2015). Sen (1988) suggested that the Deccan tholeiites with 9–10 wt% MgO are primary magmas that originated at 35–45 km depths by comparing them with available experimental data on peridotite partial melts. Sen (1995) calculated melt compositions in equilibrium with Fo_{90} olivine by adding equilibrium olivine to the highest-Mg (~7.5 wt% MgO) basalts from Western Ghats and interpreted them as primary magmas with 14–15 wt% MgO. Using the MgO and SiO_2 contents of these proposed primary magmas, Sen (1995) estimated a potential temperature of ~1400 °C. Sen and Chandrasekharam (2011) used the same approach for a picrite from Pavagadh (Gujarat) and estimated a potential temperature of ~1550 °C. Sen (1995) also estimated ~15–18% maximum melting at 100–60 km depths, similar to the estimates of White and McKenzie (1995) who used rare earth element inversion and thermodynamic constraints to conclude up to ~15% melting at 90–70 km depths and potential temperatures of ~1450–1470 °C for the Western Ghats basalts. Melluso et al. (1995) normalized the compositions of the mildly alkalic picrites of Saurashtra to 15 wt% MgO by adding equilibrium olivine and considered them as primary magmas. Using the SiO_2 and MgO values of the normalized compositions in conjunction with available thermobarometers, they calculated P–T conditions of 11–29 kbar and 1430–1468 °C for their origin. However, the P–T estimates in the above studies are highly uncertain because the primary magmas proposed by the researchers do not qualify as unmodified magmatic liquids according to phase diagram constraints (cf. Chatterjee and Sheth 2015). The phase relations are clearly evident in pseudoternary projections of the basalt tetrahedron such as the olivine-plagioclase-clinopyroxene (Ol-Pl-Cpx) projection from quartz (Qz) and the Ol-Cpx-Qz projection from Pl (Tormey et al. 1987; Grove 1993).

Most researchers agree that the picrites from Western Ghats (Mg# 0.65–0.70) do not represent liquids because their high MgO contents can be attributed to accumulations of disequilibrium olivine ($Fo_{<84}$) and clinopyroxene (Cox 1980; Beane et al. 1986; Beane and Hooper 1988; Sen 1988, 1995; Cohen and Sen 1994; Krishnamurthy et al. 2000). On the other hand, some picrites from Saurashtra (Mg# 0.66–0.80) containing crystals of $Fo_{88\text{-}92}$ olivine have

been interpreted as near-primary liquids (Krishnamurthy and Cox 1977; Melluso et al. 1995; Krishnamurthy et al. 2000; Sheth and Melluso 2008). However, Chatterjee and Sheth (2015) showed that although some Saurashtra picrites and some proposed primary magmas of the Saurashtra picrites and Western Ghats tholeiites (Sen 1995; Melluso et al. 1995) seem to plot near the 25 kbar-garnet lherzolite multiple saturation point (MSP) in the Ol-Pl-Cpx diagram, they do not plot near any MSP in the Ol-Cpx-Qz diagram. Hence, they are not melts of lherzolite. Some of Melluso et al.'s (1995) proposed primary magmas plot near the ~ 14 kbar Ol + Opx saturation boundary, indicating that these melts of garnet lherzolite may have reacted with shallower mantle to equilibrate with harzburgite (cf. Grove et al. 2013). Some other proposed primary magmas (Melluso et al. 1995; Sen and Chandrasekharam 2011) show mild silica undersaturation and higher normative Cpx contents than spinel/garnet lherzolite saturated liquids, somewhat similar to melts of pyroxenite (cf. Grove et al. 2013). The possibilities of non-lherzolitic sources are explored in the Discussion section.

Reverse fractionation modeling of primary magmas of carefully selected samples that represent liquids can reveal the P–T conditions of their last equilibration with mantle (Till et al. 2012, 2013; Grove et al. 2013; Chatterjee and Sheth 2015; Till 2017; Chatterjee 2021; Krein et al. 2021). These primary magmas rise to the crust and evolve by fractional crystallization. The goal of reverse fractionation modeling is to reconstruct the primary magma by adding back the crystallized minerals to the basalt. Mineral assemblages that crystallize from the magma depend on the pressure of crystallization. So, the first step is to determine the P–T conditions of crystallization. Clinopyroxene (augite) is ubiquitous in the Deccan basalts and alkalic rocks (Melluso et al. 1995, 2002, 2010; Simonetti et al. 1998; Dessai and Viegas 2010; Melluso and Sethna 2011; Hari et al. 2014; Krishnamurthy et al. 2014; Chatterjee and Sheth 2015; Cucciniello et al. 2015; Pande et al. 2017; Sheth et al. 2017; Dongre et al. 2018; Chatterjee 2021; Khanna et al. 2023), and thermobarometry based on clinopyroxene-liquid (Cpx-liq) equilibria and clinopyroxene composition (Putirka 2008; Neave and Putirka 2017; Higgins et al. 2022) can be conveniently used to determine their P–T of crystallization. Previous studies in selected areas suggest crystallization in the upper crust for the Deccan tholeiites (Bhattacharji et al. 1996) and in the lower crust or upper mantle (near Moho) for the Deccan alkalic rocks (Chatterjee 2021).

Reverse fractionation modeling relies on the multiple saturation points of plagioclase lherzolite (PL-MSP), spinel lherzolite (SL-MSP) and garnet-lherzolite (GL-MSP) at different pressures that are predicted by parameterized expressions of experimental data on liquids (Kinzler and Grove 1992a; Till et al. 2012; Grove et al. 2013). This study presents the results of thermobarometric calculations on picrites, basalts and alkalic rocks from a large area of the Deccan Traps, and reverse fractionation modeling on selected Deccan tholeiites including a picrite, high-Mg basalts and some low-Mg basalts, and a low-Mg mildly alkaline basalt. For samples contaminated with the continental crust, the energy-constrained coupled assimilation-fractional crystallization formulation (EC-AFC) of Spera and Bohrson (2001) and Bohrson and Spera (2001) is incorporated into the modeling. The results are used to elaborate on the mantle melting conditions and potential temperatures for Deccan volcanism.

Geological background

The Deccan Traps constitute one of the largest ($\geq$ 500,000 km^2) continental flood basalt provinces on Earth (Wadia 1975; Fig. 1). It formed by the impingement of a deep mantle plume under western India, and a hotspot track was produced by subsequent northward movement of the Indian plate (Devey and Lightfoot 1986; Mitchell and Widdowson 1991; Glišović and Forte 2017). The main Deccan sequence is exposed as thick, near-horizontal tholeiitic lava flows at the Western Ghats escarpment, roughly parallel to the Indian west coast, where the stratigraphy is well-established (Cox and Hawkesworth 1985; Beane et al. 1986; Subbarao et al. 1988; Lightfoot et al. 1990). The northwestern part of the Deccan including the Saurashtra peninsula and the Kachchh region of Gujarat consists of tholeiitic, picritic and mildly alkaline basaltic flows and dikes, and minor felsic, alkalic and carbonatitic rocks in isolated magmatic centers (Bose 1973; Krishnamurthy and Cox 1977; Melluso et al. 1995; Krishnamurthy et al. 1999; Karmalkar et al. 2000; Chatterjee and Bhattacharji 2001; Sheth and Melluso 2008; Sheth et al. 2011, 2012, 2013; Cucciniello et al. 2015, 2019, 2020; Basu et al. 2020b). There are several alkalic igneous complexes associated with the NNW-SSE oriented Barmer-Cambay Rift in the northwestern part, the ENE-WSW oriented mid-continental Narmada-Tapti Rift, and the N-S oriented western continental margin rift (Basu et al. 1993, 2020b; Dessai et al. 1990). Mildly alkaline basaltic flows are interlayered with tholeiitic flows near the western end of the Narmada-Tapti Rift (Rajpipla-Navgam area, Mahoney et al. 1985), whereas only tholeiitic flows are present farther east (Peng et al. 1998).

The Narmada-Tapti Rift and the region near the Indian west coast host two prominent dike swarms that are oriented ENE-WSW and N-S, respectively (Bhattacharji et al. 1996; Vanderkluysen et al. 2011; inset of Fig. 1). There is also a cluster of randomly oriented dikes northeast of Mumbai that cut across the lower Deccan formations of Western Ghats. In Saurashtra, E-W to ENE-WSW, NNW-SSE, NW–SE and

WNW-ESE oriented dikes are present, and the dominant E-W to ENE-WSW dikes constitute a westward extension of the Narmada-Tapti swarm (Melluso et al. 1995; Chatterjee and Bhattacharji 2001; Sheth et al. 2013; Cucciniello et al. 2015, 2020; Fig. 1). Samples from two NW-trending *en echelon* dikes exposed on the southern slope of Chotila Hill in north-central Saurashtra (Sheth et al. 2022) were studied for mineral textures and chemical composition. Chotila Hill is an erosional remnant of multiple sheet lobes of lava that overlie the Mesozoic sedimentary formations of Saurashtra Basin (Sheth et al. 2022), which in turn, rest unconformably on the Precambrian gneissic basement of Aravalli Craton (Biswas 1987; Casshyap and Aslam 1992).

Recent high-quality zircon U–Pb isotope and mineral $^{40}Ar/^{39}Ar$ age determinations indicate that the tholeiitic lavas of the Western Ghats and the region north of the Narmada-Tapti Rift erupted between ~ 66.4 Ma and ~ 65.4 Ma (Schoene et al. 2019; Sprain et al. 2019; Eddy et al. 2020). Furthermore, zircon U–Pb isotope dating indicates that the Gujarat basalts and magmatic centers formed synchronously with the Western Ghats tholeiites (Basu et al. 2020b). Older, ~ 68.6–66.8 Ma old Deccan rocks are present in some of the northern alkaline complexes ($^{40}Ar/^{39}Ar$ dates, Basu et al. 1993; Courtillot et al. 2000).

Geochemistry

Picrites (MgO 12–18 wt%, Le Bas 2000), high-Mg basalts (MgO 8–12 wt%) and high-Mg basaltic andesites (MgO > 8 wt%) are common in the lower Deccan formations such as Igatpuri, Neral and Thakurvadi of the Kalsubai Subgroup at Western Ghats (Beane et al. 1986; Beane and Hooper 1988; Peng et al. 1994; Krishnamurthy et al. 2014; Basu et al. 2020a). They are also present in the overlying formations of the Lonavala and Wai Subgroups (Beane et al. 1986; Basu et al. 2020a), and in boreholes in the southern part of Western Ghats (Khanna et al. 2023). These samples are rich in crystals of Fe-rich olivine ($Fo_{<84}$) and clinopyroxene (Cox 1980; Beane et al. 1986; Beane and Hooper 1988; Krishnamurthy et al. 2000). High-Mg basalts and picrites also occur in some Central Deccan dikes (Bondre et al. 2006; Dongre et al. 2018), and sparsely, in some flows of the Narmada-Tapti Rift and its vicinity (Mahoney et al. 1985; Peng et al. 1998). In Saurashtra, Kachchh, and Mount Pavagadh, high-Mg basalts and picrites occur in dikes and flows (Krishnamurthy and Cox 1977; Melluso et al. 1995; Sheth and Melluso 2008; Krishnamurthy et al. 2014; Cucciniello et al. 2015; Sheth et al. 2022; Fig. 1). Some of the samples such as those from Pavagadh, a Southern Saurashtra dike (D56), and flows encountered within boreholes at the western margin of Cambay Rift contain Fo_{88-92} olivine (Krishnamurthy and Cox 1977; Melluso et al. 1995; Krishnamurthy et al. 2000).

Most of the Deccan high-Mg basalts and picrites are subalkaline tholeiites (Fig. 2a, b). A few samples such as those from an Amba Dongar dike (MgO 18.6 wt%, Bhattacharji et al. 1996) and a flow from the Wadhwan borehole of Saurashtra (sample W-1, MgO 22.4 wt%, Krishnamurthy and Cox 1977) contain very high Mg and plot in the meimechite field (Le Bas 2000; Fig. 2c). A high-Mg flow from the Dhandhuka borehole (sample D-10, Krishnamurthy and Cox 1977) and two high-Mg flows (also some low-Mg flows) from the Rajpipla-Navgam section within Narmada Rift (Mahoney et al. 1985) are mildly alkaline (Fig. 2a). Based on the presence of Ti–rich augite-diopside, Melluso et al. (1995, 2006, 2010) also classified some of the Saurashtra rocks (e.g., dike samples D56 and D57) as mildly alkaline basalt. Most of the picrites and high-Mg basalts are low-Ti rocks ($TiO_2 < 1.8$ wt%, Melluso et al. 1995; Fig. 2c). High-Ti rocks are confined to northeastern Saurashtra (including the boreholes), Kachchh, Mount Pavagadh and Rajpipla-Navgam (Krishnamurthy and Cox 1977; Mahoney et al. 1985; Melluso et al. 1995; Krishnamurthy et al. 2014; Cucciniello et al. 2015). Some of the Thakurvadi samples from Western Ghats also have high Ti contents (Beane and Hooper 1988). The Chotila Hill samples BB04 and BB08 are typical examples of high-Mg, low-Ti subalkaline tholeiitic basalts (MgO ~ 11 wt%, TiO_2 ~ 1.1 wt%, Sheth et al. 2022).

The Sr–Nd isotopic compositions of picrites and high-Mg basalts from the lower Western Ghats section suggest variable degrees of crustal contamination (Peng et al. 1994; Basu et al. 2020a; Fig. 2d). Peng et al. (1994) modeled the isotopic ratios of the Kalsubai basalts through an initial stage of lower crustal contamination that generated the "common signature" basalts, and a second stage of contamination with various upper crustal components. Basu et al. (2020a) noted that all of the Kalsubai basalts with the exception of the Neral Formation basalts have broadly similar $^{87}Sr/^{86}Sr(t)$ and $\varepsilon_{Nd}(t)$ ratios. They disagreed with Peng et al.'s (1994) model and proposed that the Kalsubai basalts originated by high-degree melting of eclogitic source rocks.

The Sr–Nd isotopic compositions of the picrites and high-Mg basalts from Gujarat including Rajpipla-Navgam indicate that most of them are less contaminated than the Western Ghats picrites and high-Mg basalts (Mahoney et al. 1985; Peng and Mahoney 1995; Peng et al. 1998; Melluso et al. 2006; Cucciniello et al. 2015; Fig. 2d). Cucciniello et al. (2015) used an upper crustal contaminant (granite from western Dharwar craton) to model a maximum of ~ 12% contamination for the basalts (~ 5–8% for the high-Mg basalts and picrites) from Central Saurashtra.

The chondrite-normalized Dy_N/Yb_N ratios, sensitive to residual garnet in the mantle source, for the Western Ghats picrites and high-Mg basalts (also common low-Mg

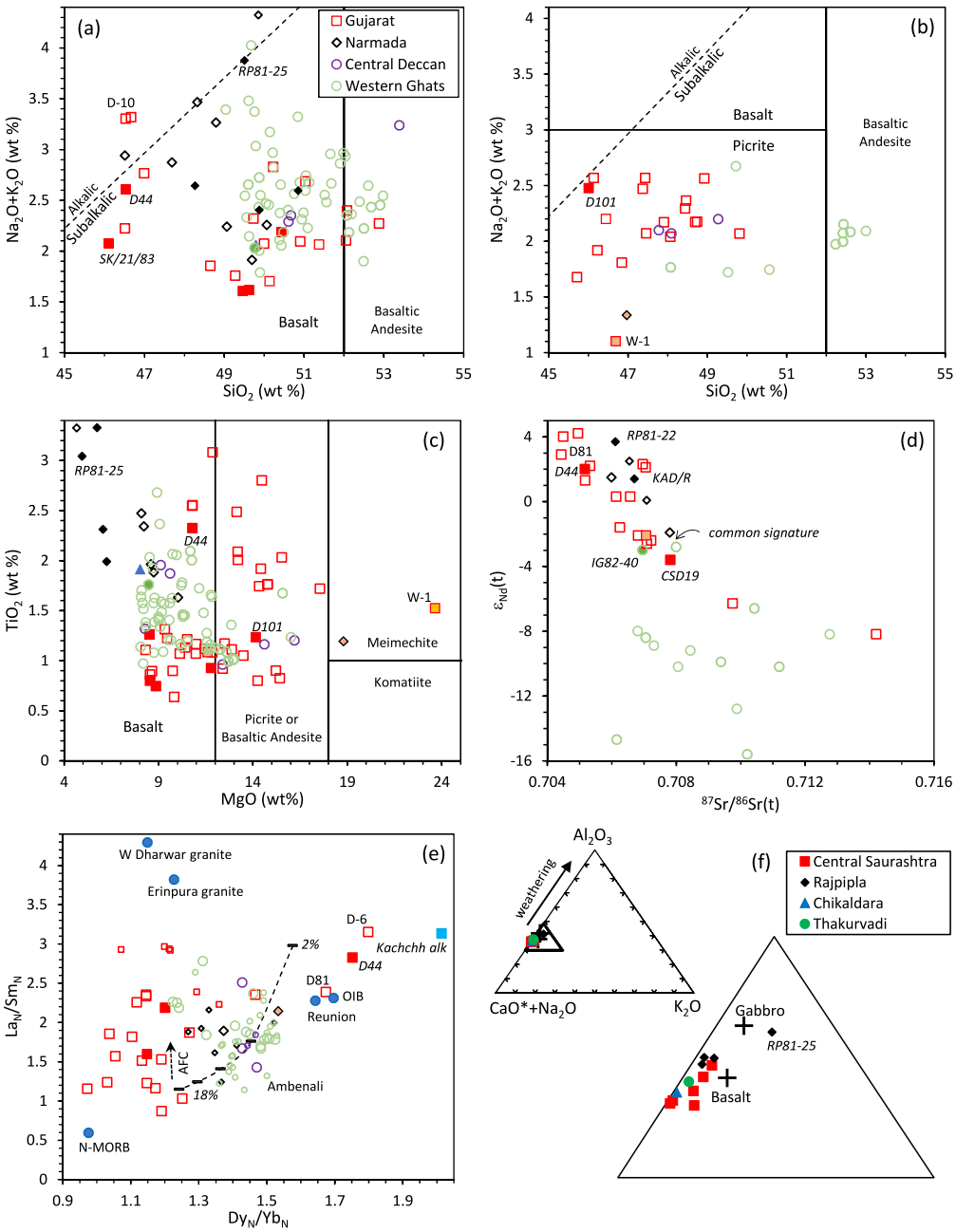

Fig. 2 Bulk composition of the Deccan picrites, high-Mg basalts, and high-Mg basaltic andesites. Some low-Mg basalts (small symbols) are also included. Filled symbols indicate samples selected for primary magma modeling. Meimechites are shown in yellow-filled symbols. Important sample numbers discussed in the text are annotated. Data sources are provided in the text. **a, b** Silica versus total alkali diagram after Le Bas et al. (1986) and Le Bas (2000) for samples with MgO contents **a** 8–12 wt%, and **b** > 12 wt%; the subalkalic-alkalic boundary is from Macdonald and Katsura (1964), **c** MgO versus TiO_2 with the meimechite-komatiite boundary from Le Bas (2000), **d** $^{87}Sr/^{86}Sr(t)$ versus $\varepsilon_{Nd}(t)$, where t is 65 Ma, **e** chondrite-normalized ratios of Dy_N/Yb_N versus La_N/Sm_N; average ratios for important basalts and granites are shown in filled blue circles (Reunion: Fisk et al. 1988, OIB and N-MORB: Sun and McDonough 1989, other sources in text) and the average ratio for the Kachchh alkaline rocks (Karmalkar et al. 2005) is shown with a filled blue square; a model batch melting curve (2–18%) for primitive spinel lherzolite (McDonough and Sun 1995; Kinzler and Grove 1992a; Kinzler 1997) is shown by a dashed line, and the direction of evolution by AFC is shown by an arrow, **f** A-CN-K ternary plot, average gabbro and basalt (plusses) from Nesbitt and Young (1982) and Babechuk et al. (2014). The triangular area demarcated in bold line in the top triangle is expanded in the bottom triangle

basalts, Peng et al. 1994; Sheth et al. 2014; Basu et al. 2020a; Khanna et al. 2023) are similar to < 18% batch melts of spinel lherzolite, consistent with the melting estimates in previous studies (Sen 1995; White and McKenzie 1995; Chatterjee and Sheth 2015; Fig. 2e). In comparison, the higher Dy_N/Yb_N ratios of average OIB (Sun and McDonough 1989), Reunion basalts (Fisk et al. 1988), Kachchh alkaline rocks (Bhuj plugs, Karmalkar et al. 2005), Mount Pavagadh picrites (Melluso et al. 1995), and samples from the Saurashtra boreholes (e.g., D-6, Peng and Mahoney 1995) and some dikes (D44, Melluso et al. 2006) indicate that they possibly originated through melting of a garnet-bearing mantle. In general, most of the picrites and high-Mg basalts from Saurashtra (Melluso et al. 1995, 2006; Cucciniello et al. 2015) have lower Dy_N/Yb_N ratios (< 1.3) compared to Western Ghats. The La_N/Sm_N ratios of the Saurashtra rocks indicate mixing of the spinel lherzolite melts with granite (Erinpura, De Wall et al. 2021; Western Dharwar, Jayananda et al. 2006), consistent with the isotopic data.

Petrography and mineral chemistry

A large number of mineral analyses on Deccan picrites, basalts and alkaline rocks are available in the literature (Melluso et al. 1995, 2002, 2010; Simonetti et al. 1998; Dessai and Viegas 2010; Melluso and Sethna 2011; Hari et al. 2014; Krishnamurthy et al. 2014; Chatterjee and Sheth 2015; Cucciniello et al. 2015; Pande et al. 2017; Sheth et al. 2017; Dongre et al. 2018; Chatterjee 2021; Khanna et al. 2023). The Chotila Hill high-Mg basalts BB04 and BB08 were analyzed on a JEOL JXA-8200 Superprobe electron probe microanalyzer (EPMA) at Massachusetts Institute of Technology, Cambridge, MA, USA, using an accelerating voltage of 15 kV, a 10 nA beam current, and 1–10 µm beam diameter (see Methods in Supplementary file for more information). For mineral analysis, the counting times were 20–40 s per element, and the 1σ standard deviations of accumulated counts were 0.3–1.0% for major elements and 1–5% for minor elements. Matrix corrections were carried out using the CITZAF package (Armstrong 1995).

The Chotila Hill samples consist of elongated laths and skeletal crystals of plagioclase, phenocrysts of olivine and clinopyroxene, and a fine-grained interstitial groundmass comprising dendritic Fe-rich clinopyroxene, olivine, albite, and spinel (Fig. 3). Vesicles are rare. They are small, spherical and filled with smectitic clay (saponite), a common low-temperature alteration product in Deccan basalts (Chatterjee and Sheth 2015; Fig. 3c). Rare orthopyroxene is present in sample BB04 (Fig. 3d). The olivine phenocrysts are rounded by alteration, although some euhedral grains are present in sample BB08 (Fig. 3e). The alteration also consists of saponite that occurs as rinds and veins cutting through the crystals. Inclusions of plagioclase and melt with small clinopyroxene crystals are present in the olivine phenocrysts.

The clinopyroxene phenocrysts in the Chotila Hill samples are augite, and their compositions ($En_{49-44}Fs_{11-14}Wo_{38-43}$, Mg# 0.64–0.80 Table 1, Table S1) are within the diopside-ferroaugite range for clinopyroxenes in the Saurashtra and Mount Pavagadh high-Mg basalts and picrites (Krishnamurthy and Cox 1977; Melluso et al. 1995; Melluso and Sethna 2011; Krishnamurthy et al. 2014; Cucciniello et al. 2015; Fig. 4a). They are also similar to the augite in Rajpipla basalts (Krishnamurthy et al. 2014). In comparison, the augite in Western Ghats picrites and high-Mg basalts are relatively Mg-rich (Krishnamurthy et al. 2014; Chatterjee and Sheth 2015; Fig. 4a). Melluso et al. (2010) reported spinel-hosted inclusions of diopside with high jadeite content ($Jd_{<6}$) and Mg-rich augite in Southern Saurashtra dikes D56 and D57 (Fig. 4a, b). Diopside with high aegirine and jadeite contents (cf. Morimoto et al. 1988) also occur in the Deccan alkalic rocks, but this variety of diopside has very high wollastonite contents (Simonetti et al. 1998; Melluso et al. 2002; Dessai and Viegas 2010; Hari et al. 2014; Pande et al. 2017; Sheth et al. 2017; Chatterjee 2021; Fig. 4a, b).

The composition of olivine phenocrysts in the Chotila Hill samples is Fo_{84-87} (Table 1). In comparison, the forsterite content of olivine in the Central Saurashtra picritic dikes is somewhat lower (Fo_{71-84}, Melluso et al. 1995; Cucciniello et al. 2015), and as noted above, those in the Pavagadh and Southern Saurashtra dikes and flows are higher (Fo_{88-92}, Krishnamurthy and Cox 1977; Melluso et al. 1995; Krishnamurthy et al. 2000). The orthopyroxene in sample BB04 has a composition of $En_{84}Fs_{12}Wo_4$ (Mg# 0.87) that is more Mg-rich than the orthopyroxene (or pigeonite) in other Central Saurashtra samples and samples from Pavagadh, Rajpipla and Western Ghats (Melluso et al. 2010; Krishnamurthy et al. 2014; Chatterjee and Sheth 2015; Cucciniello et al. 2015; Fig. 4a). The plagioclase in the Chotila Hill samples has compositions of $An_{71-63}Ab_{28-35}Or_{1-2}$. Plagioclase with higher anorthite contents are present in the Central Saurashtra picrites (An_{72-82}, Cucciniello et al. 2015). Chromite contains substantial amounts of Mg (0.42–0.57 apfu) and Fe^{3+} (0.07–0.18 apfu), and has Cr/(Cr + Al) ratios of 0.58–0.59. Chromite and magnetite-ilmenite are also present in the Central Saurashtra picrites (Cucciniello et al. 2015).

P–T of crystallization

The P–T of crystallization of the Deccan picrites, basalts and alkalic rocks were determined using clinopyroxene compositions including those analyzed in this study, and bulk compositions where the clinopyroxene is in equilibrium (Mahoney et al. 1985; Melluso et al. 1995, 2010; Simonetti

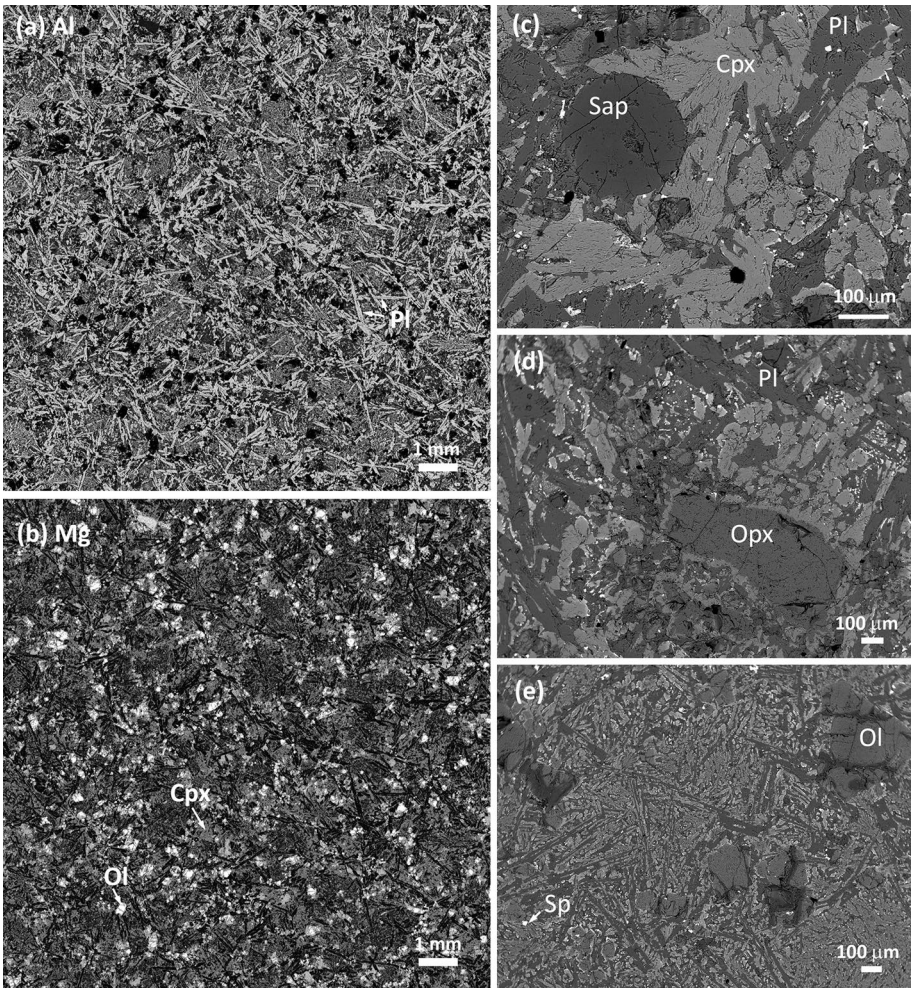

Fig. 3 **a, b** Al and Mg x-ray elemental maps of sample BB04. Note acicular plagioclase in (**a**). The olivine phenocrysts appear bright and the Cpx phenocrysts are of intermediate shade in (**b**). **c–e** BSE images of samples BB04 (**d**) and BB08 (**c** and **e**). Abbreviations: *Ol* Olivine, *Pl* Plagioclase, *Cpx* Clinopyroxene, *Opx* Orthopyroxene, *Sp* Spinel, *Sap* Saponite

et al. 1998; Melluso and Sethna 2011; Krishnamurthy et al. 2014; Chatterjee and Sheth 2015; Cucciniello et al. 2015; Vijayan et al. 2016; Pande et al. 2017; Sheth et al. 2017; Dongre et al. 2018; Chatterjee 2021; Khanna et al. 2023). Before the thermobarometric calculations were performed, the entire clinopyroxene dataset was filtered according to the recommendations of Neave and Putirka (2017). Clinopyroxene analyses with cation sums outside the 4.00 ± 0.02 range and $Jd < 0.01$ calculated on a six-oxygen (6O) basis (Fig. 4c) according to Putirka (2008) were discarded. In an atomic Ca/(Ca + Mg + Fe) versus Al diagram (6O basis, Fig. 4d), each group of Deccan clinopyroxenes occurring in the tholeiites (especially the Central Saurashtra group) shows two compositional trends similar to Icelandic clinopyroxenes (Neave and Putirka 2017) that are characterized by variable Al at high Ca/(Ca + Mg + Fe) and variable Ca/(Ca + Mg + Fe) at low Al. These trends can be attributed to sector zoning formed at low degrees of undercooling, and the low-Al sectors are believed to form by Ca and Al dilution as a result of disequilibrium incorporation of Mg and Fe (Neave and Putirka 2017, and references therein). Therefore, all clinopyroxene analyses from the tholeiites with Al (6O basis) < 0.11 (Fig. 4d) were also excluded. The clinopyroxenes in the Deccan alkalic rocks show concentric zoning (Chatterjee 2021; Pande et al. 2017) and little variation in Ca/(Ca + Mg + Fe) (Fig. 4d). Ubide et al. (2019) and Macdonald et al. (2023) concluded that all clinopyroxenes from alkali basalts irrespective of zoning patterns may record equilibrium. Hence, all clinopyroxenes from the Deccan alkalic rocks were considered in the P–T calculations.

Clinopyroxene-liquid thermobarometry

The clinopyroxene-liquid (Cpx-liq) barometer of Neave and Putirka (2017) along with the P-dependent thermometric expression (Eq. 33) of Putirka (2008) is suitable for determining the P–T of crystallization of the Deccan rocks. This thermobarometer has a standard error of estimate of ± 1.4 kbar and ± 27 °C, and it is valid between pressures of 1 bar and 20 kbar, temperatures > 1100 °C, and oxygen fugacity < 1.5 log unit above the quartz-fayalite-magnetite

Table 1 Average composition of minerals in the Chotila Hill high-Mg basalts

Sample	BB04					BB08				
	Ol	Cpx	Opx	Pl	Sap	Ol	Cpx	Pl	Sp	Sap
Weight percent										
SiO_2	39.61	50.55	53.50	51.58	53.63	40.12	49.54	52.49	0.12	50.19
TiO_2	0.01	0.87	0.16		0.02	0.00	1.13		0.73	0.07
Al_2O_3	0.04	3.63	2.61	29.62	2.34	0.05	4.69	28.60	20.13	4.60
Cr_2O_3	0.11	0.34	0.92		0.05	0.08	0.24		42.20	0.03
Fe_2O_3		0.92	0.82				0.36		5.97	
FeO	14.18	7.97	7.61	0.71	9.86	14.11	11.01	0.89	19.13	9.55
MnO	0.20	0.21	0.19		0.06	0.13	0.24		0.23	0.02
MgO	45.48	15.78	30.01	0.37	23.94	45.57	14.57	0.50	10.52	23.66
CaO	0.26	18.68	2.04	13.62	0.58	0.23	17.29	13.32	0.14	1.08
Na_2O		0.21	0.04	3.42	0.21		0.17	3.66		0.29
K_2O		0.00	0.01	0.21	0.17		0.02	0.24		0.20
NiO	0.18					0.21			0.06	
ZnO									0.06	
Total	100.1	99.2	97.9	99.5	90.8	100.5	99.3	99.7	99.3	89.7
Ratios and endmembers										
Mg#	0.851	0.762	0.865		0.812	0.852	0.696			0.815
Jd		1.0	0.2				1.2			
Ae		0.6	0.1				0.2			
En		46.9	83.9				43.9			
Fs		13.3	11.9				18.6			
Wo		39.9	4.1				37.5			
An				67.9				65.9		
Ab				30.8				32.7		
Or				1.2				1.4		

All analyses are averages of 10 points

Ol Olivine, *Cpx* Clinopyroxene, *Opx* Orthopyroxene, *Pl* Plagioclase, *Sap* Saponite, *Sp* Spinel, *Jd* Jadeite, *Ae* Aegirine, *En* Enstatite, *Fs* Ferrosilite, *Wo* Wollastonite, *An* Anorthite, *Ab*: Albite, *Or* Orthoclase

buffer (ΔQFM < 1.5) (Neave et al. 2019). Coexisting magnetite-ilmenite pairs in Central Saurashtra samples CSD8 and CSD9 (Cucciniello et al. 2015) yield log(fO_2) values of −15.1 at 829 °C (ΔQFM = −1.2) and -15.9 at 719 °C (ΔQFM = 0.54) with the QUILF program (Andersen and Lindsley 1988), and similar log(fO_2) values have been estimated for many Saurashtra and Pavagadh rocks (Melluso et al. 1995; Melluso and Sethna 2011; Sheth and Melluso 2008; Cucciniello et al. 2015). Hence, the log(fO_2) values are appropriate for application of the Cpx-liq thermobarometer of Neave and Putirka (2017).

The Cpx-liq thermobarometer can only be applied if Cpx is in equilibrium with the bulk (considered as liquid). Neave et al. (2019) recommend that for Cpx and bulk to be in equilibrium, the Fe^T-Mg exchange coefficient, Cpx-liq $K_D(Fe^T\text{-Mg})$, must be within ± 0.03 of the value predicted by Eq. 35 of Putirka (2008), and the observed values of the DiHd, EnFs and CaTs components of Cpx must be within ± 0.06, ± 0.05 and ± 0.03 of predicted values (references in Putirka 2008). An inspection of the data set indicates that the above conditions of equilibrium are rarely satisfied for the Deccan rocks (Fig. 5a, b). For example, the K_D values for the Chotila Hill samples are between 0.47 and 1.01, much higher than the equilibrium value of 0.27 ± 0.03 predicted by Eq. 35 of Putirka (2008). The alkalic rocks of Sarnu-Barmer and Mundwara are exceptions with many clinopyroxenes showing equilibrium K_D values (0.24–0.30, Chatterjee 2021; Vijayan et al. 2016; Simonetti et al. 1998; Pande et al. 2017; Fig. 5a). The only tholeiites that show equilibrium K_D values are the Pavagadh picrite D97 (0.30, Melluso et al. 1995), Central Saurashtra high-Mg basalt D44 (0.26, Melluso et al. 1995) and Rajpipla low-Mg basalt RT-1 (0.26, Mahoney et al. 1985; Krishnamurthy et al. 2014). The observed and predicted values of the DiHd and EnFs components of Cpx for these alkalic and tholeiitic rocks are also well correlated (Fig. 5c, the CaTs components are very low and not shown). The similar calculated P–T of crystallization for D97 (3.4 kbar/1161 °C) and RT-1 (3.0 kbar/1159 °C) indicate upper crustal conditions, and the slightly negative pressure for D44 (-0.6 kbar/1139 °C) probably indicates

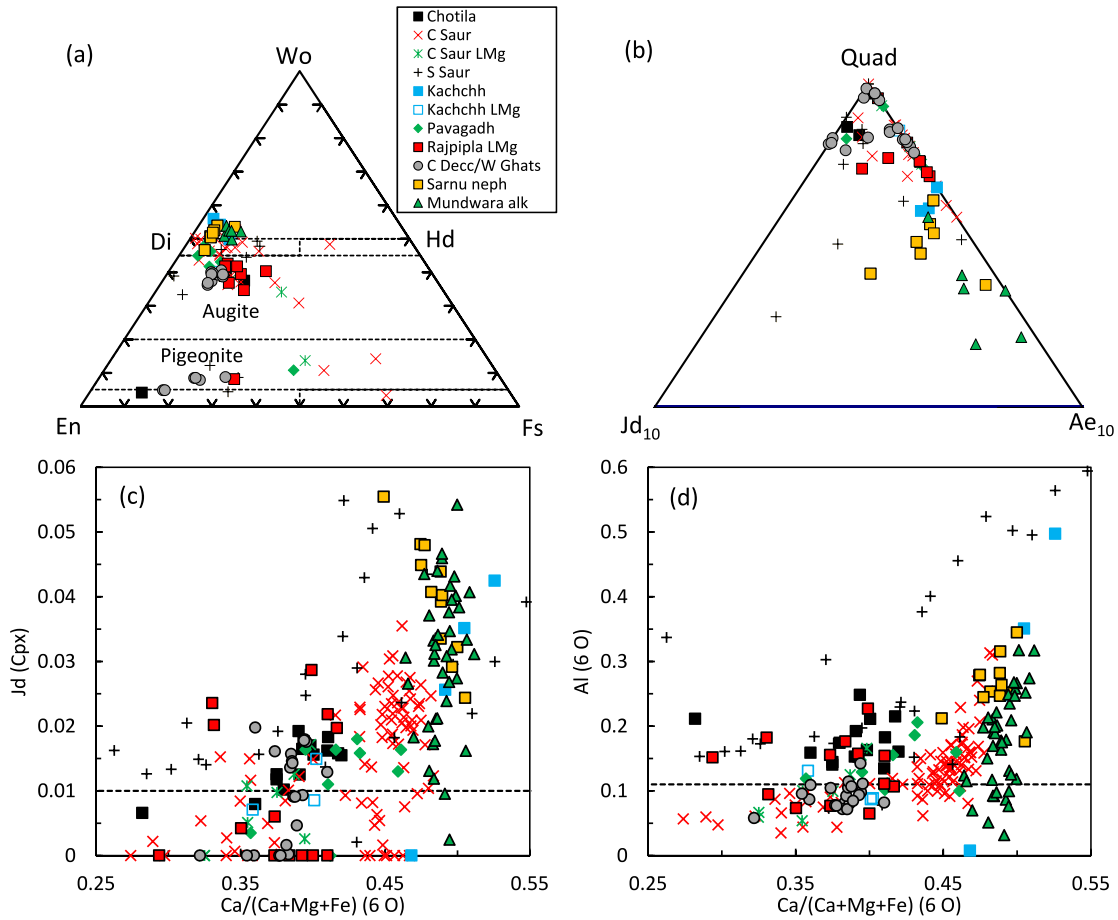

Fig. 4 Compositions of pyroxene in the Deccan picrites, high-Mg basalts, low-Mg (LMg) basalts, and alkalic rocks plotted after **a, b** Morimoto et al. (1988), and **c, d** after Neave and Putirka (2017). The data sources are discussed in the text, except for Chotila Hill (this study)

very shallow, subsurface conditions (Fig. 6a, Table S1). Thus, the P–T of crystallization for the high-Mg and the low-Mg basalts are similar. The P–T for the Sarnu-Barmer (8.7–11.7 kbar/1226–1264 °C) and the Mundwara (1.7–8.6 kbar/1117–1151 °C) alkalic rocks are variable with the maximum pressures far exceeding those of the tholeiites (Fig. 6a, Table S1). Higher pressures for the same Sarnu-Barmer samples (12.2–15.5 kbar/1250–1284 °C) and similar P–T for the same Mundwara samples (3.7–8.8 kbar/1134–1148 °C) were calculated by Chatterjee (2021) using the same thermometric expression (Eq. 33) and older barometric expressions (Eqs. 30 and 31) of Putirka (2008).

Clinopyroxene thermobarometry

In the absence of Cpx-liq equilibrium in most samples, thermobarometers based only on clinopyroxene composition (Eqs. 32a,d of Putirka 2008; Higgins et al. 2022) were applied to determine the P–T of crystallization of the Deccan rocks. Putirka's (2008) formulations are based on multiple regression of clinopyroxene compositions in basalt obtained from experiments in the P–T range of 1 bar-75 kbar and 800–2200 °C. The quoted uncertainties are ± 3.1 kbar and ± 58 °C. Higgins et al.'s (2022) formulations are based on random forest machine learning-based algorithms that provide independent estimates of the uncertainties in P and T. This thermobarometer also uses clinopyroxene compositions in basalt obtained from experiments in the P–T range of 2 bar-30 kbar and 750–1250 °C.

For the Chotila Hill samples, Putirka's (2008) formulations register P–T conditions of 4.0–6.1 kbar/1165–1200 °C for BB04, and 4.5–7.5 kbar/1148–1179 °C for BB08 (Fig. 6b, Table S1). The P–T for most Deccan tholeiites including high-Mg and low-Mg basalts are 0.1–6.1 kbar/1047–1221 °C (excluding negative pressure results) with only two clinopyroxenes yielding 7.5–7.9 kbar pressures (Fig. 6b). The P–T for the spinel-hosted Cpx inclusions in samples D56 and D57 (Melluso et al. 2010) are notably high (7.0–12.7 kbar/1150–1289 °C, one outlier at 1067 °C, Fig. 6b, Table S1). These pressures

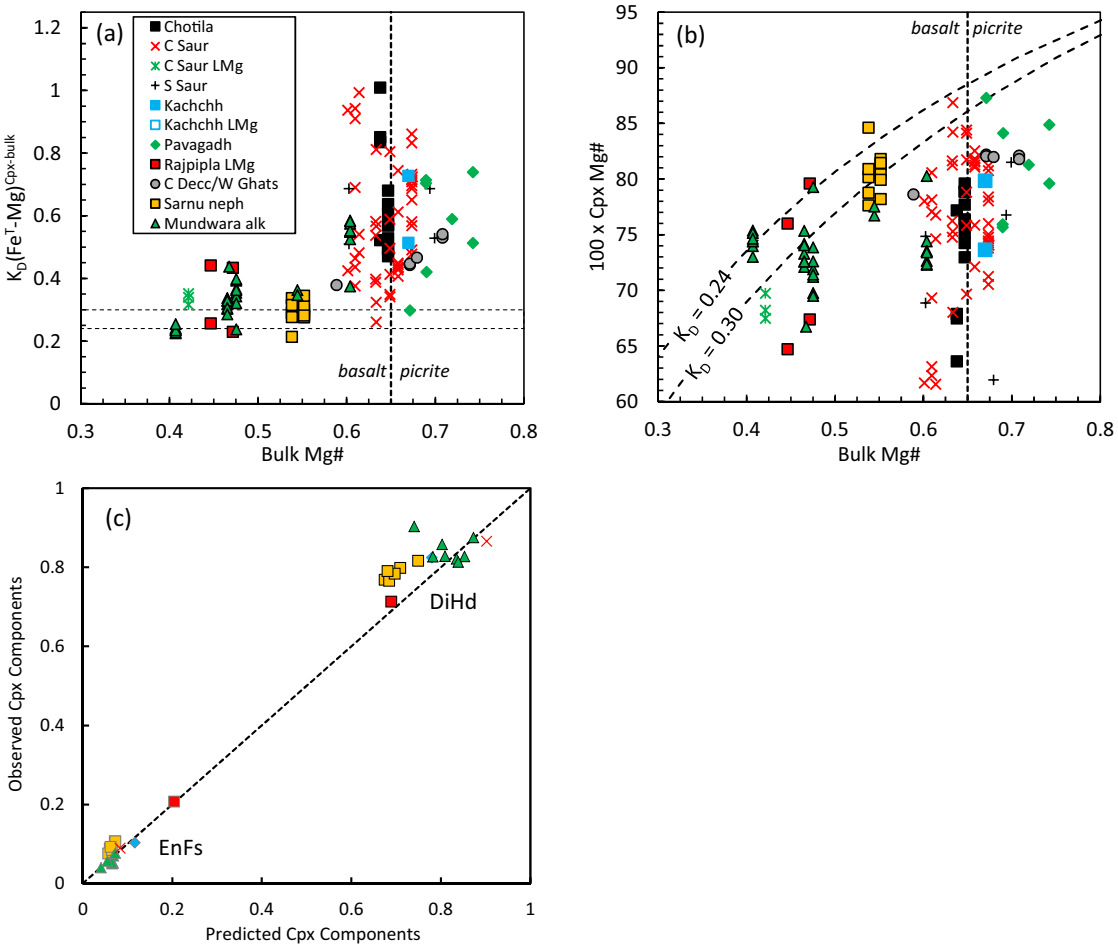

Fig. 5 **a,b** Bulk Mg# versus **a** clinopyroxene-bulk Fe^T-Mg distribution coefficient, and **b** Cpx Mg#; the equilibrium clinopyroxenes plot between the two dashed lines. **c** Correlation of the observed Cpx components (DiHd and EnFs, calculated from Cpx analyses) versus predicted Cpx components of the equilibrium clinopyroxenes in (**a, b**) according to the methods of Putirka (2008) and Neave and Putirka (2017)

are even higher than the pressures for the Sarnu-Barmer (1.3–8.2 kbar/1035–1205 °C) and Mundwara (0.4–7.7 kbar/978–1129 °C) alkalic rocks. The thermobarometer of Higgins et al. (2022) registers similar pressures but lower temperatures, the reason for which is unclear (Fig. 6c, Table S1).

Compared to the P–T determined using Cpx-liq equilibria (Neave and Putirka 2017), the P–T determined using only Cpx composition (Putirka 2008) are lower by 3.5–7.4 kbar and 70–190 °C for the Sarnu-Barmer alkalic rocks, and the temperatures are lower by 20–150 °C for the Mundwara alkalic rocks (Fig. 6a, b), as also found by Chatterjee (2021). However, the P–T for the Rajpipla tholeiite RT-1 using the same formulations are similar (Cpx-liq equilibria: 3 kbar/1159 °C; Cpx composition: 4.0–6.1 kbar/1147–1169 °C). The pressures for the tholeiite samples RT-1 (low-Mg basalt), and D44 and D97 (high-Mg basalts) using the formulations of Neave and Putirka (2017) (3 kbar, −0.6 kbar and 3.4 kbar) and Higgins et al. (2022) (3.4–4.1 kbar, 2.1 kbar and 2.2 kbar) are also similar (Table S1). Thus, the P–T calculated for the Deccan tholeiites using only Cpx compositions (Putirka 2008) are reliable, and there is no significant difference in the P–T of crystallization for the high-Mg and the low-Mg basalts.

Primary magma modeling

Calculation methods

At low pressures in the upper crust, where plagioclase lherzolite (PL, Ol + Pl + Cpx + Opx) is stable, primitive basaltic liquids fractionate with decreasing temperature and evolve by crystallizing olivine, followed by Ol + Pl, and then by Ol + Pl + Cpx under nominally anhydrous conditions (Kinzler and Grove 1992a; Grove et al. 1992;

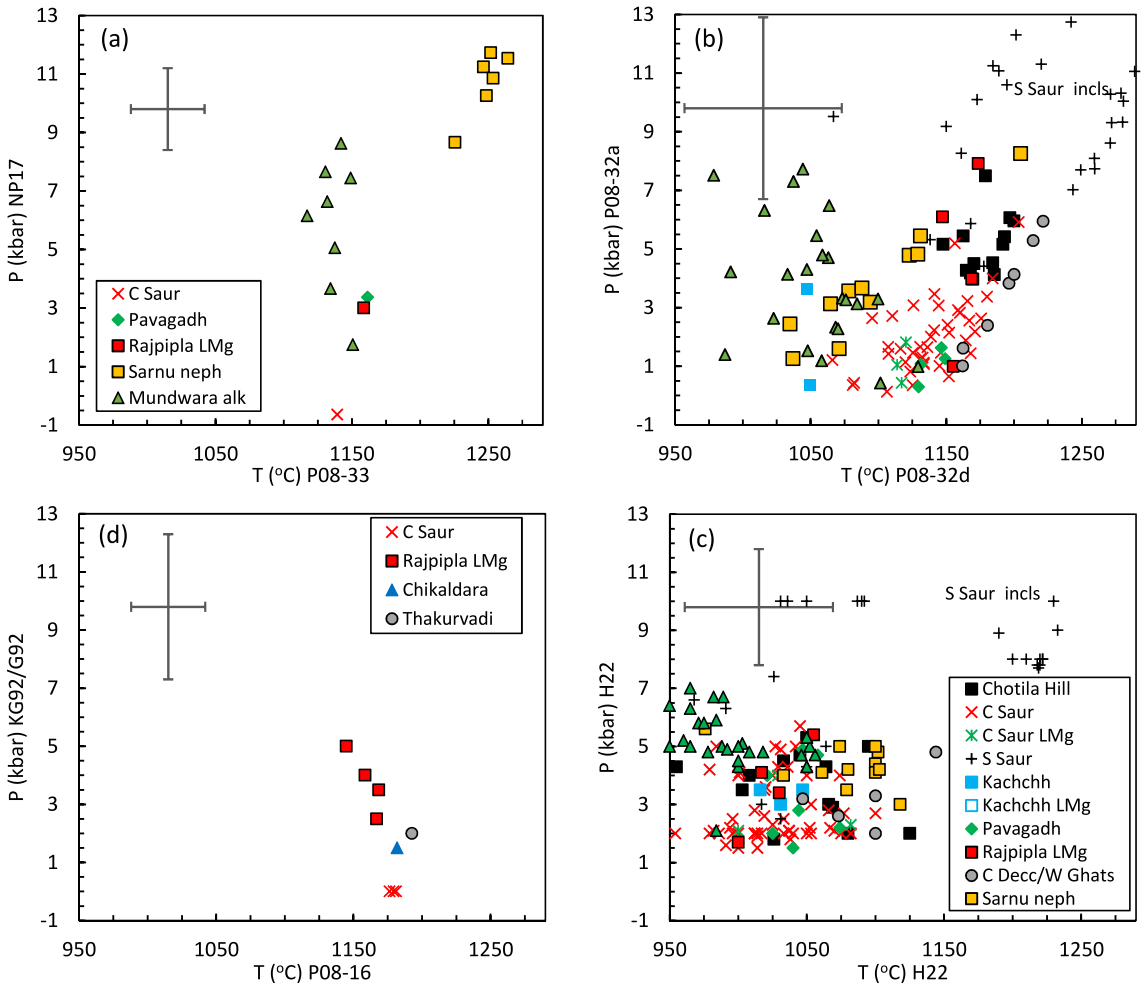

Fig. 6 P–T of crystallization of the Deccan picrites, high-Mg basalts, low-Mg (LMg) basalts, and alkalic rocks based on **a** Cpx-liquid equilibria, **b, c** Cpx composition, **d** liquid composition. P08: Putirka (2008), Eqs. 16, 32a,d and 33; NP17: Neave and Putirka (2017); H22: Higgins et al. (2022); KG92: Kinzler and Grove (1992b); G92: Grove et al. (1992). The error bars at the top left corner of each panel represent the average uncertainties in the calculated pressures and temperatures

Yang et al. 1996). These authors have provided detailed descriptions of the low-pressure phase relationships using Ol-Cpx-Qz and Ol-Pl-Cpx pseudoternary diagrams. At higher pressures near the Moho, plagioclase crystallization is suppressed and the evolving liquid crystallizes Ol + Cpx after an initial stage of Ol crystallization (Villiger et al. 2004). Silica-undersaturated, nepheline-normative liquids plot at negative values of Qz in the Ol-Cpx-Qz projection, and the evolving liquid moves away from the Qz apex as it crystallizes Ol + Cpx.

The composition of the primary magma of a basalt and its P–T of last equilibration with mantle are calculated by backtracking along the fractionation path in reverse (Reverse FC method, Chatterjee and Sheth 2015; Krein et al. 2021; Chatterjee and Ghose 2023; Chatterjee 2023). The calculations involve determining the parental liquid composition at each step of reverse fractionation until the final liquid is at its high-pressure SL-MSP or GL-MSP predicted by the expressions of Till et al. (2012) and Grove et al. (2013). Mineral-liquid equilibrium is ensured by maintaining equilibrium Fe–Mg distribution for Ol-liq ($K_D(Fe^T\text{-}Mg) = 0.3$, Roeder and Emslie 1970) and Cpx-liquid ($K_D(Fe^T\text{-}Mg) = 0.25$, Grove et al. 1992), and equilibrium Ca-Na distribution for plagioclase-liquid (Grove et al. 1992) (the effect of uncertainties in the K_D values are discussed below). This method was followed to model the primary magmas of the Deccan basalts assuming a lherzolitic source. The possibility of an origin from a hybrid lherzolite source containing non-lherzolitic components such as pyroxenite, hornblendite and eclogite is explored in the Discussion section.

For simultaneous fractional crystallization and assimilation (Reverse EC-AFC method, Chatterjee 2023), the energy-constrained AFC formulation of Spera

and Bohrson (2001) and Bohrson and Spera (2001) was incorporated in the modeling. The solidus and liquidus of the upper crustal assimilant (900 °C and 1000 °C) and the energy parameters used in the calculations were as in Table 1 of Bohrson and Spera (2001), and the equilibration temperature (T_{eq}) was set at 1000 °C. The gneiss-melt partition coefficient for K was estimated from the average contents of K in upper crustal gneiss and its melt (Ahmad et al. 2016; De Wall et al. 2022; Jayananda et al. 2006, 2018). The basalt-melt partition coefficient for K was estimated from the phase proportions in the reverse fractionation model and mineral-melt partition coefficients, which are close to zero except for plagioclase ($D_K^{Pl-melt} = 0.13$, Bindeman et al. 1998).

Because thermobarometric calculations indicate crystallization of the Deccan tholeiites in the upper crust, an upper crustal assimilant was used in the Reverse EC-AFC modeling. Cucciniello et al. (2015) also used an upper crustal contaminant for the Central Saurashtra basalts. Some authors suggest that the upper crustal material may have been previously subducted to deeper levels, and the contamination process may have occurred within a modified upper mantle or lower crust (Melluso et al. 2006). Other authors prefer a lower crustal contamination with amphibolite for the lower formation Western Ghats basalts (Peng et al. 1994). For the purpose of comparison, the primary magma of a Western Ghats sample was also modeled with amphibolite as an assimilant at an assumed lower crustal pressure of 8 kbar. The amphibolite-melt partition coefficient for K was from Rushmer (1991), the amphibolite solidus and liquidus were set at 950 °C and 1100 °C, and the lower crustal energy parameters were from Table 2 of Bohrson and Spera (2001).

Sample selection

A critical first step in primary magma modeling is to determine whether the bulk composition of the sample represents a liquid. The sample should not be altered by weathering, and it should not contain accumulations of disequilibrium crystals. An unaltered liquid would plot on its fractionation path in the pseudoternary diagrams. A sample that plots on its Ol-Pl-Cpx cotectic boundary, which is a point that approximately coincides with the PL-MSP at a specific pressure in the Ol-Pl-Cpx projection, is considered a liquid. However, if the sample plots on its olivine control line, it is not possible to ascertain *a priori* if it represents a liquid. If it is indeed a liquid, its primary magma modeled through reverse fractionation of olivine must plot on its high-pressure MSP for lherzolite or lherzolite modified by other lithologies.

The Deccan basalts and picrites with published compositions (Krishnamurthy and Cox 1977; Mahoney et al. 1985; Beane et al. 1986; Beane and Hooper 1988; Peng et al. 1994, 1998; Melluso et al. 1995; Bondre et al. 2006; Krishnamurthy et al. 2014; Cucciniello et al. 2015; Basu et al. 2020a; Sheth et al. 2022; Khanna et al. 2023) were plotted in the pseudoternary diagrams (Fig. 7). To evaluate whether these basalts and picrites represent liquids, each sample was separately plotted along with its cotectic boundaries and MSPs in the pseudoternary diagrams (not shown). Among the high-Mg basalts and picrites, only three from Central Saurashtra (CSD2, CSD4 and CSD19, Cucciniello et al. 2015), one from near Tapti Rift (CH83-32, Peng et al. 1998), and one from Western Ghats (IG82-40, Peng et al. 1994) qualify as liquids that crystallized at low pressures. These five high-Mg basalts, three additional very high-Mg basalts and picrite that plot on the olivine control line, and four low-Mg basalts discussed below plot close to the average unaltered basalt in an A-CN-K ternary diagram (Nesbitt

Table 2 Average P–T conditions of crystallization of the selected Deccan picrite and basalts and P–T of last equilibration of their primary magmas with mantle

	Crystallization		Primary magma			
	P (kbar)	T (°C)	P (kbar)	±	T (°C)	±
D101			30.0	2.0	1513	17
SK/21/83			24.5	3.5	1452	34
D44			35.5	4.5	1531	38
CSD2	0.001	1174	11.5	2.9	1313	39
CSD4	0.001	1179	12.0	3.0	1318	40
CSD19	0.001	1177	11.3	2.8	1310	39
CH83-32	1.5	1179	12.0	3.0	1320	40
IG82-40	2	1190	12.3	3.1	1322	40
RT-1	3.5	1166	9.5	2.4	1289	39
KAD-R	2.5	1164	10.8	2.7	1303	39
RP81-22	4	1156	13.3	3.3	1333	40
RP81-25	5	1144	12.8	3.2	1322	40

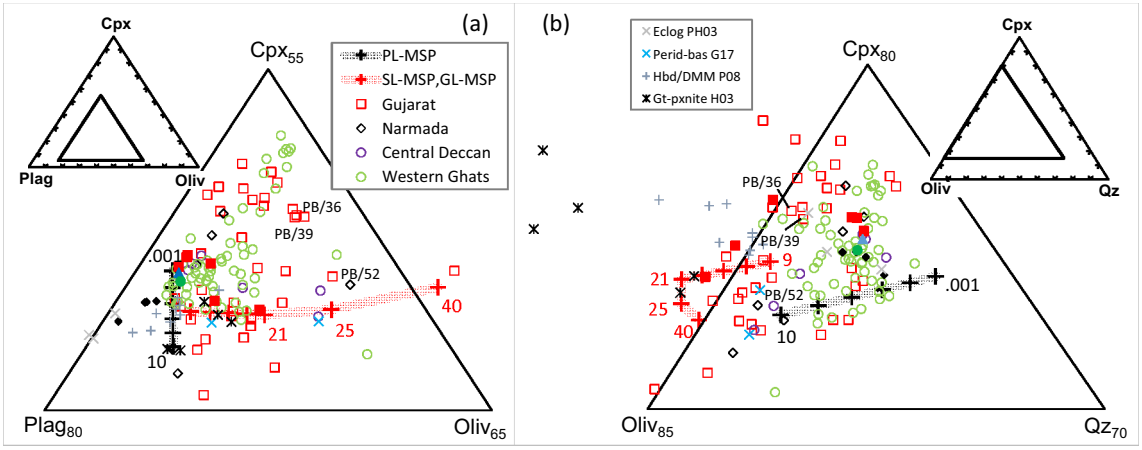

Fig. 7 Bulk composition of the Deccan high-Mg basalts, picrites, and some low-Mg basalts plotted in Ol-Pl-Cpx and Ol-Cpx-Qz pseudoternary projections from Qz and Pl, respectively, according to the methods of Tormey et al. (1987) and Grove (1993). The data sources are discussed in the text. Low-Mg basalts are shown by small symbols, and the samples selected for primary magma modeling are shown by filled symbols. Also shown are the average PL-MSPs at 1 bar-10 kbar pressures in 2 kbar intervals (Kinzler and Grove 1992a), SL-MSPs at 9–21 kbar pressures in 3 kbar intervals (Till et al. 2012), and GL-MSP at 25 kbar and 40 kbar pressures (Grove et al. 2013). Only the average MSPs are shown for clarity. Experimentally generated melts of garnet pyroxenite (H03, 20–25 kbar, 14–67% melting, Hirschmann et al. 2003), hornblendite-depleted MORB mantle mixture (P08, 15 kbar, 27–43% melting, Pilet et al. 2008), eclogite (PH03, 20–30 kbar, 60–87% melting, Pertermann and Hirschmann 2003) and fertile peridotite + MORB (G17, 29 kbar, 1500–1540 °C, Gao et al. 2017) are shown for comparison

and Young 1982; Babechuk et al. 2014; Fig. 2f), indicating that they are not significantly altered by weathering. Samples CSD2 and CSD4 are from an ENE-trending dike, and CSD19 is from a NW-trending dike (Cucciniello et al. 2015). These are low-Ti tholeiites with 0.8–1.2 wt% TiO_2 (Fig. 2c, Table S2). Sample CH83-32 is a high-Ti tholeiite (1.9 wt% TiO_2, Fig. 2c, Table S2) from the middle of the Chikaldara section, south of the eastern part of Tapti Rift (Peng et al. 1998). Sample IG82-40 is also a high-Ti tholeiite (1.8 wt% TiO_2, Fig. 2c, Table S2) from the Thakurvadi Formation of the Kalsubai Subgroup in the lower part of Western Ghats (Peng et al. 1994). Among the low-Mg tholeiitic flows associated with high-Mg tholeiitic flows and interlayered with alkalic flows at Rajpipla-Navgam (Mahoney et al. 1985), three tholeiitic basalts (KAD/R, RT-1 and RP81-22) and a mildly alkaline basalt (RP81-25) are slightly displaced from their Ol-Pl-Cpx cotectic boundaries into the plagioclase stability field (Fig. 7a, small filled black symbols). These samples represent liquids that are slightly modified by excess plagioclase accumulation. Their bulk compositions were corrected by subtracting 1.5–7.5% plagioclase so that they plotted on their respective Ol-Pl-Cpx cotectic boundaries. These are high-Ti basalts (2.0–3.3 wt% TiO_2, Mahoney et al. 1985; Fig. 2c) and RP81-25 is potassic (1.29 wt% K_2O, Table S2). They have lower CaO contents (9.9–11.3 wt%) and higher P_2O_5 contents (0.22–0.41 wt%) than the high-Mg basalts. The five high-Mg basalts and four low-Mg basalts discussed above plot on their Ol-Pl-Cpx cotectic boundaries at pressures of 1 bar-2 kbar and 2.5–5.0 kbar, respectively (Fig. 6d, 8a, c, Table S2). The temperature of crystallization for the high-Mg and low-Mg basalts are 1174–1190 °C and 1144–1166 °C, respectively, with uncertainties of ± 27 °C (Eq. 16, Putirka 2008). These P–T conditions are similar to the P–T obtained from Cpx-liq and Cpx composition thermobarometry (Neave and Putirka 2017; Putirka 2008; Fig. 6). The remarkable agreement in the P–T calculated for sample RT-1 with the three methods (Cpx-liq equilibria: 3 kbar/1159 °C; Cpx composition: 4.0–6.1 kbar/1147–1169 °C, and liquid composition: 3.5 kbar/1169 °C, Table S1) indicates that the P–T results are robust and reliable. Hence, the primary magmas of the nine selected high-Mg and low-Mg samples were calculated using low-pressure reverse fractionation methods.

In addition to the nine samples discussed above, samples that are displaced from the Ol-Pl-Cpx cotectic boundary toward the olivine apex in the pseudoternary projections (Fig. 7) and whose modeled primary magmas plot on their high-pressure lherzolite MSP (see modeling section) represent liquids on the olivine control line. Only two very high-Mg basalts (MgO 10.7–11.6 wt%, samples D44 and SK/21/83, Melluso et al. 1995; Krishnamurthy et al. 2014) and a picrite (MgO 14 wt%, sample D101, Melluso et al. 2006) qualify as liquids on the olivine control line. Sample D44 is from a Central Saurashtra high-Ti dike that contains augite, plagioclase and spinel, and Cpx is in equilibrium with the bulk (Melluso et al. 1995; Fig. 2c, 6, Table S2). Sample D101 containing olivine, augite and spinel (Melluso and Sethna 2011) and sample SK/21/83 (Mount Girnar) are

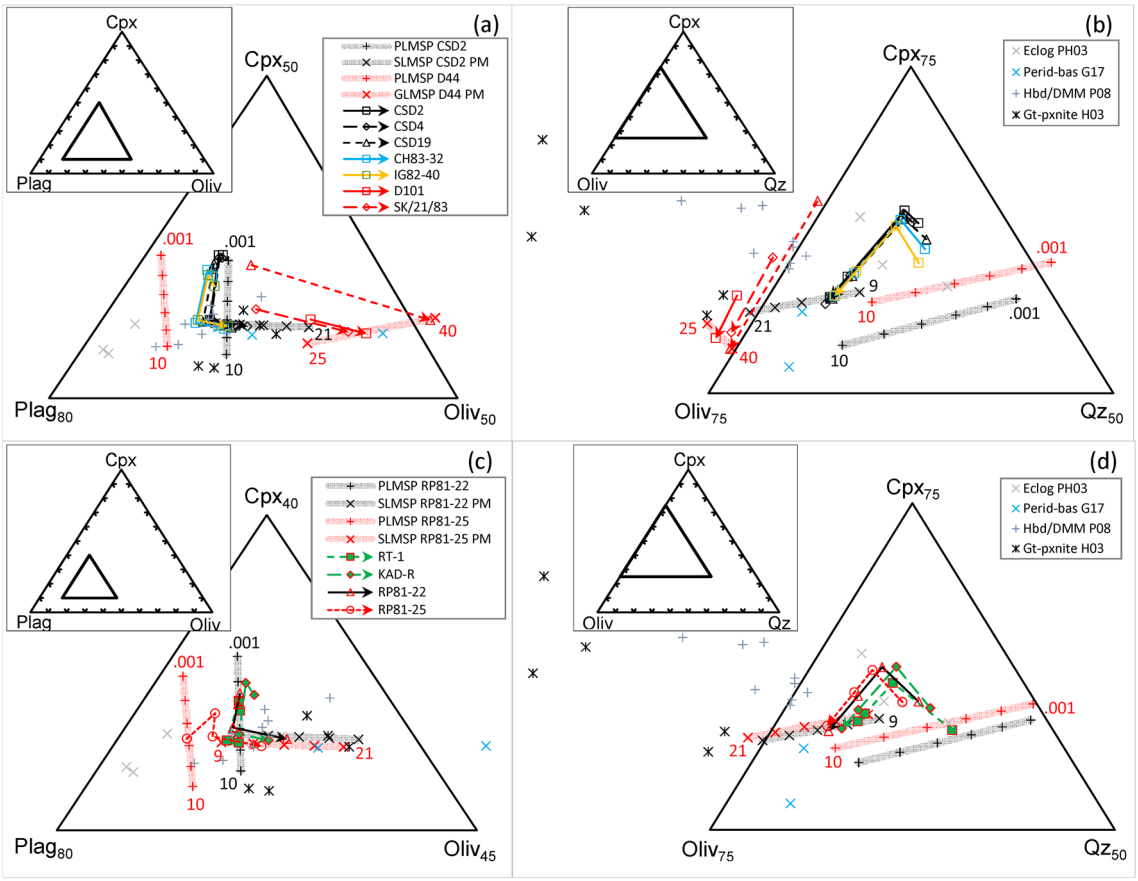

Fig. 8 Ol-Pl-Cpx and Ol-Cpx-Qz pseudoternary projections from Qz and Pl, respectively, with the composition of the selected Deccan **a, b** high-Mg basalts and picrite, and **c, d** low-Mg basalts and their calculated parental and primary magmas (modeled without spinel) plotted according to Tormey et al. (1987) and Grove (1993). The reverse fractionation path for each sample is shown by a line with arrowhead. Except for the very high-Mg basalts and picrite, each line is connected by four symbols starting with the sample followed by its parental liquids at the first appearance of clinopyroxene, plagioclase and olivine. The symbol at the arrowhead represents the primary magma. The PL-MSPs at 1 bar-10 kbar in 2 kbar intervals (Kinzler and Grove 1992a) for **a, b** samples CSD2 and D44, and **c, d** samples RP81-22 and RP81-25 are shown by plusses. The SL-MSPs at 9–21 kbar in 3 kbar intervals (Till et al. 2012) and GL-MSPs at 25 kbar and 40 kbar (Grove et al. 2013) for the corresponding primary magmas (PM) are shown by crosses. The sources for the experimentally derived melts are as in Fig. 7

from low-Ti dikes in Southern Saurashtra (Fig. 2c, Table S2). These samples have high alkali contents, but they plot in the basalt field and below the alkalic-subalkalic boundary of Macdonald and Katsura (1964) (Fig. 2a). According to the scheme of Tormey et al. (1987) and Grove (1993), they are nepheline-normative and plot in the silica undersaturated part of the Ol-Cpx-Qz pseudoternary diagram (Fig. 8).

The Nd–Sr isotopic compositions of the Saurashtra high-Mg basalts such as sample CSD19 indicate moderate degrees of contamination by the upper crust (with two exceptions, Cucciniello et al. 2015; Fig. 2d). The Thakurvadi high-Mg basalt IG82-40 has a similar Nd–Sr isotopic composition to sample CSD19 and "common signature" basalts (Fig. 2d), for which a lower crustal contaminant has been suggested (Peng et al. 1994). However, IG82-40 plots on its 2-kbar Ol-Pl-Cpx cotectic boundary (Fig. 8a), indicating that it evolved in the upper crust. In some Deccan formations, the primitive high-Mg basalts are more contaminated than the evolved basalts, and this observation has been used to argue against an AFC process and to propose that the contaminated isotopic signatures were acquired before the onset of basaltic differentiation (Cox and Hawkesworth 1984, 1985; Basu et al. 2020a). However, the modeling in this study deals with the formation of the primitive high-Mg basalts from their primary magmas, which is assumed to have occurred through AFC involving assimilation of wall rocks from the magma conduits. Therefore, the primary magmas of the five high-Mg basalts plotting on the Ol-Pl-Cpx cotectic boundary were modeled using the low-pressure Reverse EC-AFC method (Chatterjee 2023). An average Aravalli Banded Gneiss (Ahmad et al. 2016) for the Central Saurashtra samples, and an average

Western Dharwar TTG gneiss (Jayananda et al. 2018) for the Chikaldara and Thakurvadi samples were used as upper crustal assimilants in the calculations. For comparison, the primary magma of the Thakurvadi sample was also modeled using an average Western Dharwar amphibolite (Naqvi et al. 1983) as a lower crustal assimilant.

The Rajpipla-Navgam alkalic and tholeiitic rocks overlap and form a well-correlated array in an $^{87}Sr/^{86}Sr(t)$ versus $\varepsilon_{Nd}(t)$ plot, indicating mixing of high-$\varepsilon_{Nd}(t)$ basalts with an LILE-enriched low-$\varepsilon_{Nd}(t)$ mantle endmember (Mahoney et al. 1985). There is no indication of significant crustal contamination, especially in samples RP81-22 and KAD/R (Fig. 2d). Therefore, the primary magmas of the four selected low-Mg basalts were modeled with the Reverse FC method. Sample D44 also has high $\varepsilon_{Nd}(t)$ and low $^{87}Sr/^{86}Sr(t)$ ratios (Melluso et al. 2006; Fig. 2d), indicating that it is uncontaminated by the crust. Hence, the primary magmas of the very high-Mg basalts D44 and SK/21/83, and the picrite D101 were also modeled using the Reverse-FC method.

Results

Low-pressure reverse fractionation modeling shows that the Ol-Pl-Cpx saturated high-Mg basalts were last equilibrated with spinel lherzolite at P–T conditions of 12–13 kbar and 1321–1333 °C (Fig. 8a,b, Table S2). They crystallized in the upper crust that was at a temperature of 792–830 °C when the basaltic melts intruded. The melts began to crystallize at temperatures of 1238–1252 °C, and upper crustal assimilation started when the basaltic liquids were at 1177–1202 °C. The maximum M_a*/M_c ratios were between 0.06 and 0.29 that resulted in 1–6% contamination of the basalts (Table S2). The high-Mg basalts are 41–53% fractionated. During olivine crystallization, the liquids fractionated by ~ 3–5%, Mg# decreased from 0.73 to 0.70–0.71, and SiO_2, Al_2O_3, CaO and Na_2O increased (Fig. 9). During Ol + Pl crystallization, the liquids fractionated by ~ 20–27%, Mg# decreased to 0.63–0.66, SiO_2, CaO and Na_2O continued to increase, whereas Al_2O_3 decreased (Fig. 9). During Ol + Pl + Cpx crystallization, the liquids fractionated by ~ 11–27%, Mg# decreased to 0.54–0.60, SiO_2 and Na_2O increased further, whereas CaO decreased along with Al_2O_3 (Fig. 9).

The Ol-Pl-Cpx saturated low-Mg basalts of Rajpipla-Navgam were last equilibrated with spinel lherzolite at P–T of 10–14 kbar and 1296–1337 °C (Fig. 8c,d, Table S2). They are 63–67% fractionated, and the fractionation was dominated by Ol + Pl + Cpx crystallization. During olivine crystallization, the liquids fractionated by ~ 1–5%, and Mg# decreased from 0.73 to 0.70–0.72. During Ol + Pl crystallization, the liquids fractionated by ~ 9–18%, and Mg# decreased to 0.67–0.69. During Ol + Pl + Cpx crystallization, the liquids fractionated by ~ 42–51%, and Mg# decreased to 0.42–0.47. The oxide variation trends are the same as for the Ol-Pl-Cpx saturated high-Mg basalts (Fig. 9).

The very high-Mg basalts and picrite plotting on the olivine control line were last equilibrated with garnet lherzolite at P–T of 28–40 kbar and 1486–1569 °C (Fig. 8a, b, Table S2). They originated by 9–25% fractional crystallization of olivine. During fractionation, the Mg# decreased from 0.72–0.76 to 0.63–0.68 as SiO_2, Al_2O_3, CaO and Na_2O increased (Fig. 9). For sample SK/23/83, forward extrapolation of the olivine control line intersects the Ol-Pl cotectic boundary at a pressure of ~ 4 kbar, indicating that it crystallized in the upper crust (Fig. 8a). On the other hand, the extrapolations of the olivine control lines for D44 intersect the Ol-Cpx cotectic boundary (near the Ol-Cpx-Pl cotectic boundary), indicating relatively higher pressures of crystallization (Fig. 8a). The calculated Ni contents of all modeled Deccan primary magmas are consistent with the Ni contents predicted by the fertile lherzolite melting model of Herzberg et al. (2016) (Fig. 9i).

For a hypothetical lower crustal EC-AFC of the Thakurvadi high-Mg basalt IG82-40 at an assumed pressure of 8 kbar, a primary magma equilibrated with garnet lherzolite at ~ 40 kbar/1593 °C would evolve by crystallizing 23% olivine, 11% Ol + Cpx and 12% Ol + Cpx + Pl to generate the sample. The primary melt would begin to crystallize at 1382 °C, assimilation of lower crust preheated to 898 °C would start at 1274 °C, and the sample would become 12.6% contaminated. These results are very different from the results for upper crustal EC-AFC that indicate a primary magma equilibrated with spinel lherzolite at 12 kbar/1318 °C beginning to crystallize at 1252 °C and assimilating upper crust (preheated to 828 °C) at 1202 °C, resulting in 5.1% contamination (Fig. 8a, b, Table S2). The P–T of equilibration with garnet lherzolite in the lower crustal EC-AFC model is similar to the P–T for the Saurashtra very high-Mg basalt D44. However, unless there is demonstrable evidence of lower crustal fractionation for the Thakurvadi sample, the upper crustal EC-AFC model is preferable.

Uncertainties

The above modeling results do not consider spinel as a crystallizing phase. Melluso et al. (2010) concluded that spinel is a common phase that co-crystallized with olivine in the Deccan basalts. Spinel crystallizes over a short interval and the total mass of Cr-spinel is very small (< 1 wt%, Till et al. 2012; Krein et al. 2021). Furthermore, bulk Cr contents are not available for most samples. Hence Cr-spinel was not considered in the modeling. The effect of adding aluminous spinel on the P–T of equilibration with mantle was considered. Adding equilibrium olivine and spinel (spinel-liquid $K_D(Fe^T\text{-}Mg) = 0.95$, Elkins-Tanton and Grove 2003)

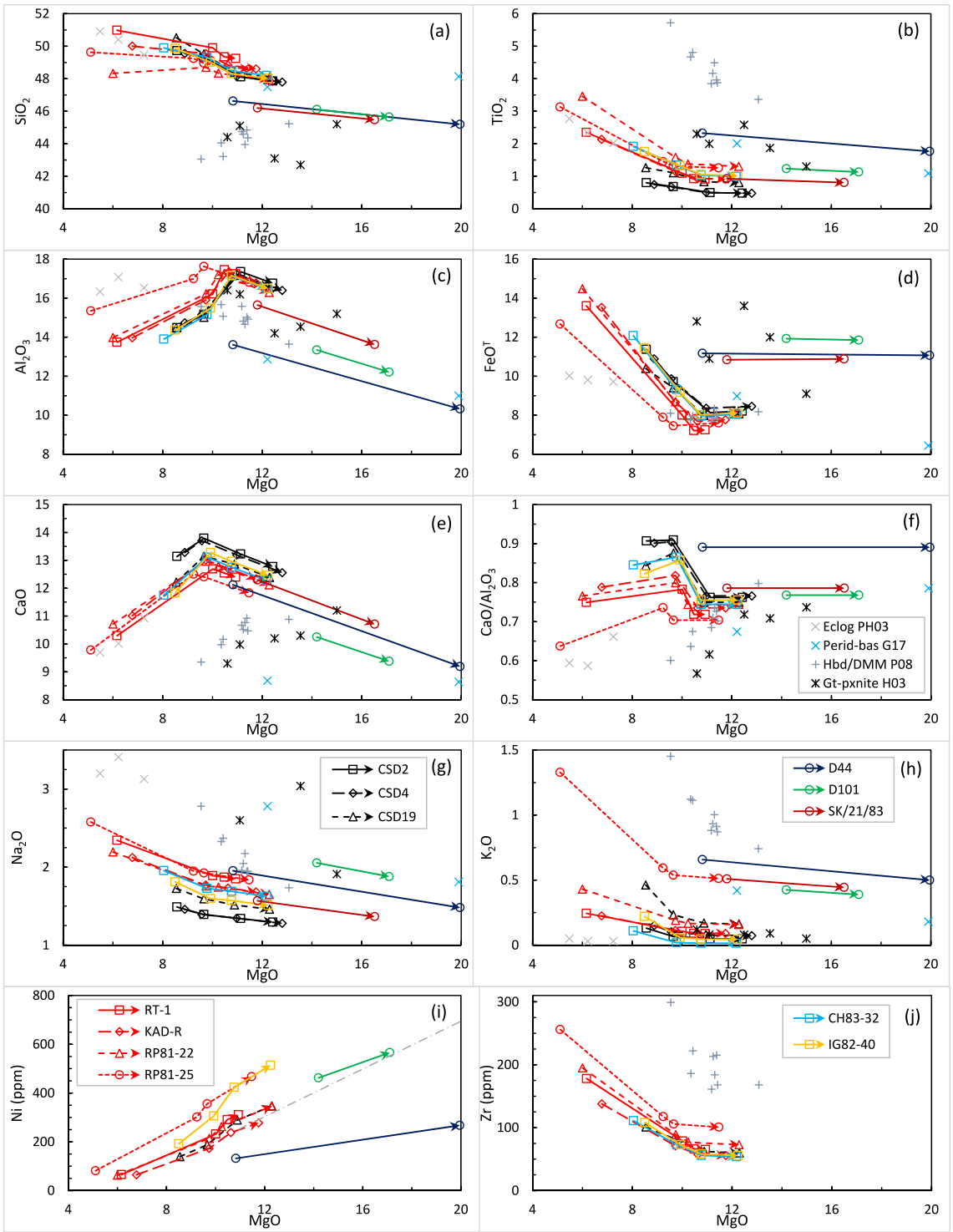

Fig. 9 Bivariate plots showing the variation of the major and minor oxides (wt%), the CaO/Al_2O_3 ratio, and Ni and Zr (ppm) with MgO (wt%) for the selected Deccan picrite, and high-Mg and low-Mg basalts, and their parental and primary magmas (modeled without spinel, see legend in **g-j**). The fractionation paths are as described in Fig. 8. The sources for the experimentally derived melts (see legend in **f**) are as in Fig. 7. The grey dash-dot line in (i) represents the trend of predicted Ni contents in the Deccan primary magmas according to the fertile lherzolite melting model of Herzberg et al. (2016)

in 9:1 ratio in Stage 3 of the modeling does not significantly affect the estimated P–T for the primary magma of basalts that equilibrated with the mantle at shallow depths (pressures changed by −0.5 kbar to 1.5 kbar). However, spinel addition significantly decreases the P–T of equilibration for the very high-Mg basalts and picrite, whose P–T are lowered by 1–6 kbar and 8–50 °C.

The parameterized expressions that predict the lherzolite MSPs (Kinzler and Grove 1992a; Till et al. 2012; Grove et al. 2013) and the plotting algorithm for the pseudoternary projections (Tormey et al. 1987; Grove 1993) are all based on the bulk total-Fe content, implicitly assuming $Fe^{2+} = Fe^{T}$. This is because the experiments on which the expressions are based do not report Fe^{3+} contents. Hence, the modeling in the above section was carried out assuming $Fe^{2+} = Fe^{T}$. The presence of Fe^{3+} lowers the olivine-liquid equilibrium $K_D(Fe^{T}\text{-}Mg)$ (Blundy et al. 2020). For $Fe^{2+} = 0.85Fe^{T}$, the olivine-liquid equilibrium $K_D(Fe^{T}\text{-}Mg)$ is 0.27 (Blundy et al. 2020), which is at the lower limit of the 0.30 ± 0.03 value recommended by Roeder and Emslie (1970). During fractional crystallization, Fe^{3+} is incorporated into spinel and clinopyroxene. The effect on the P–T of equilibration with mantle considering $Fe^{2+} = 0.85Fe^{T}$, appropriate for the log(fO_2) values of Deccan basalts, was explored using Canil and O'Neill's (1996) data for the incorporation of Fe^{3+} in spinel and clinopyroxene (Table S3, Fig. S1, S2). This further lowered the P–T by 3–4 kbar/25–42 °C for the very high-Mg basalts and picrite, and by 0.5–2 kbar/8–27 °C for the other samples.

Uncertainties in the estimated compositions and P–T of primary magmas arise from the uncertainties in the equilibrium values of the mineral-liquid $K_D(Fe^{T}\text{-}Mg)$ coefficients. A ± 10% change in the Ol-liquid and Cpx-liquid equilibrium $K_D(Fe^{T}\text{-}Mg)$ values results in a change of about ± 3% in MgO and ± 6% in FeO for samples that require the highest degrees of reverse fractionation. Another source of uncertainty is the composition of the mantle minerals with which the primary magmas are assumed to equilibrate. These uncertainties are greater than those based on uncertainties in the equilibrium mineral-liquid $K_D(Fe^{T}\text{-}Mg)$ coefficients. The primary magmas in equilibrium with olivine in the $Fo_{88\text{-}92}$ composition range have uncertainties of ± 6% in Mg#, ± 12% in MgO, ± 9% in FeO, ± 25% in pressure, and ± 3% in temperature. The uncertainties in P–T are similar to the ± 3 kbar and ± 30 °C uncertainties of the reverse fractionation method (Krein et al. 2021). However, the uncertainties in P–T for the very high-Mg basalts and picrite are up to ± 5 kbar and ± 40 °C. Considering all factors, the best estimates of P–T of last equilibration with mantle are 25–36 ± 5 kbar/1452–1531 ± 40 °C for the very high-Mg basalts and picrite, and 10–13 ± 3 kbar/1289–1333 ± 40 °C for the other samples (Table 2).

Discussion

P–T of crystallization

Clinopyroxene composition thermobarometry (Putirka 2008) indicates that most Deccan tholeiites including the high-Mg and the low-Mg basalts crystallized at P–T conditions of 0.1–6.1 kbar and 1047–1221 °C with only two clinopyroxenes showing higher pressures (7.5–7.9 kbar, Fig. 6b). These two clinopyroxenes are small Ti–Al-rich ($TiO_2 > 1.3$ wt%, $Al_2O_3 > 5.2$ wt%) groundmass grains from low-Ti, high-Mg tholeiite BB08 (Chotila Hill) and high-Ti, low-Mg tholeiite KAD/R (Rajpipla). Krishnamurthy et al. (2014) noted the compositional similarity of the clinopyroxene in KAD/R with the clinopyroxenes in mildly alkaline basalts from Navgam, and concluded that KAD/R represents a mixed liquid of tholeiitic and alkalic components. According to Krishnamurthy et al. (2014), such mixing occurred between high-Ti tholeiitic and alkalic liquids at Rajpipla-Navgam, Central Kachchh and Pavagadh. The occurrence of high-Ti–Al clinopyroxenes in the low-Ti, high-Mg tholeiites of Chotila Hill and Southern Saurashtra (inclusions in spinel in samples D56 and D57, Melluso et al. 2010) indicates that mixing between low-Ti tholeiitic liquids and alkalic liquids may have also occurred. The spinel-hosted clinopyroxenes in D56 and D57 yield very high P–T conditions of crystallization (7.0–12.7 kbar/1150–1289 °C, one outlier at 1067 °C) that are even higher than the P–T for the high-Ti–Al clinopyroxenes in Sarnu-Barmer (1.3–8.2 kbar/1035–1205 °C) and Mundwara (0.4–7.7 kbar/978–1129 °C) alkalic rocks. Evidently, the clinopyroxenes of alkalic affinity crystallized over a large range of pressure (0.4–12.7 kbar). Furthermore, because the pressures determined for the Sarnu-Barmer alkalic rocks using clinopyroxene compositions are lower by 3.5–7.4 kbar than the more reliable pressures determined using Cpx-liq equilibria (this study; Chatterjee 2021), the actual crystallization pressures for the alkalic clinopyroxenes may be even higher than 12.7 kbar.

Although there is some uncertainty in the pressures calculated using only clinopyroxene compositions for the alkalic rocks, they are reliable for the tholeiites that contain clinopyroxenes (augite) with relatively lower amounts non-quadrilateral components. For example, the Rajpipla tholeiite RT-1 with clinopyroxene containing 0.9 wt% TiO_2 and 3.5 wt% Al_2O_3 (Krishnamurthy et al. 2014) yields remarkably similar P–T conditions using Cpx-liq equilibrium (3 kbar/1159 °C), Cpx composition (4 kbar/1169 °C) and liquid composition (2 kbar/1157 °C, Table S1). Thus, it can be concluded that the crystallization pressures for all Deccan tholeiites (42

high-Mg and low-Mg samples from different parts of the Deccan Traps, Table S1) are less than ~ 6 kbar.

Krishnamurthy et al. (2014) considered the Pavagadh picrites (PB/36, PB/39 and PB/52) as primitive liquids with suspended phenocrysts, and suggested that the picrites would crystallize Ol + Pl to reach the Ol-Pl-Cpx cotectic boundary at a low pressure. They arrived at this conclusion by plotting the bulk compositions of the picrites in an Ol-Cpx-Qz pseudoternary diagram using an incorrect projection scheme (Grove et al. 1982). Nevertheless, low-pressure crystallization of the Pavagadh picrites is supported by the P–T estimates in this study for the above-mentioned samples (0.3–1.6 kbar/1130–1149 °C) based on clinopyroxene compositions, and for sample D97 (3.4 kbar/1161 °C) based on Cpx-liq equilibria (Table S1). Thus, the Deccan picrites, like the high-Mg and low-Mg tholeiites, also crystallized at low pressures. However, the Ol-Pl-Cpx pseudoternary diagram plotted according to the corrected scheme of Grove (1993) shows that crystallization of Ol + Pl as suggested by Krishnamurthy et al. (2014) will move the bulk compositions away from the Ol-Pl-Cpx cotectic boundary at all pressures, whereas removal of Ol + Cpx will move the compositions toward the Ol-Pl-Cpx cotectic boundary (Fig. 7a). Although this may indicate a relatively high pressure of crystallization, there is no such evidence from clinopyroxene compositions, and the picrite-hosted olivine and clinopyroxene crystals are in disequilibrium with the bulk (mineral-bulk $K_D(Fe^T\text{-}Mg) = 0.51–0.91$ for Cpx, and 0.22 and 0.34–0.85 for olivine, Krishnamurthy et al. 2000, 2014). In addition, the high Mg#s of the picrites (0.69–0.74) imply that they may be primary melts of the mantle, and yet, they do not show multiple saturation with lherzolite at any pressure (Fig. 7). Therefore, the Pavagadh samples do not represent liquids, and their picritic bulk compositions are a result of large accumulations of disequilibrium olivine and clinopyroxene crystals. This does not preclude a deep mantle source for their origin, and Krishnamurthy et al.'s (2014) estimated > 20 kbar pressure for their origin may be correct. Indeed, the Pavagadh picrite sample D81 (Melluso et al. 2006) as well as the Saurashtra borehole samples such as D-6 (Peng and Mahoney 1995) have high, OIB-like Dy_N/Yb_N ratios (Fig. 2e) that indicate their possible origin from deep garnet-bearing sources.

Krishnamurthy et al.'s (2014) alkaline picrite samples from Kachchh, KB/11/83 and KB/13/83, plot in the basanite field of the total alkali-silica diagram (Le Bas et al. 1986) (not shown). These samples and the very high-Mg tholeiite sample SK/21/83 from Mount Girnar (Krishnamurthy et al. 2014) plot at negative quartz values in the Ol-Cpx-Qz pseudoternary diagram of this study (Fig. 8b), indicating that they are silica-undersaturated rocks. The trend of the down-temperature olivine crystallization path of sample SK/21/83 indicates that is crystallized at upper crustal pressures (Fig. 8a). On the other hand, the Bhuj (Kachchh) alkalic rocks that originated by melting of carbonated garnet lherzolite, crystallized near the Moho (~ 12 kbar/1120–1160 °C, Chatterjee 2021). Thus, the maximum pressures of crystallization for the alkalic rocks (> 12.7 kbar, 12 samples including samples with spinel-hosted Cpx inclusions, Table S1) are much greater than the maximum pressures of crystallization for the tholeiites (~ 6 kbar).

Mantle sources

High-pressure pyroxenite melting experiments (Kogiso et al. 2004; Hirschmann et al. 2003) indicate the presence of a thermal divide that separates SiO_2-poor melts from SiO_2-rich melts. The SiO_2-poor melts are olivine-normative and they plot on the SiO_2-undersaturated side of the thermal divide in pseudoternary diagrams. Both the SiO_2-undersaturated and the SiO_2-rich melts plot far away from their spinel or garnet MSPs predicted by the expressions of Till et al. (2012) and Grove et al. (2013) and the evolved SiO_2-undersaturated melts plot on their Ol + Cpx + garnet/spinel saturation boundaries (Grove et al. 2013). Experimentally derived melts of carbonated garnet lherzolite are also strongly SiO_2-undersaturated (Grove et al. 2013; Chatterjee 2021). Although a few Deccan picrites and very high-Mg basalts show mild SiO_2-undersaturation (Fig. 7), the samples whose primary magmas were modeled have higher CaO/Al_2O_3 ratios and SiO_2 contents than all of the experimentally derived pyroxenite melts (Fig. 9). Furthermore, olivine addition moves the Deccan picrite and very high-Mg basalts toward the olivine apex and away from the experimentally derived melts of pyroxenite in the pseudoternary diagrams (Fig. 8a,b). Hence, it is unlikely that the Deccan picrites and very high-Mg basalts originated by melting of pyroxenite or carbonated lherzolite. Melts of hornblendite and depleted MORB mantle mixtures (Pilet et al. 2008) are mostly SiO_2-undersaturated and relatively high in the plagioclase component (Fig. 8), They do not overlap with the model fractionation paths of the Deccan samples. Thus, an origin of the Deccan rocks by melting of a hornblendite-enriched mantle source can be precluded. Gao et al. (2017) conducted high-pressure experiments on layered peridotite + MORB mixtures and found picritic and komatiitic melts (12.2 wt% and 19.9 wt% MgO) in two of their runs at 29 kbar and above the dry peridotite solidus. The picritic melt plots somewhat close to the model primary magmas of the Deccan high-Mg basalts (Fig. 8a, b). However, its lower CaO and Al_2O_3 contents and CaO/Al_2O_3 ratios, and higher Na_2O contents (Fig. 9) indicate that an eclogite-enriched mantle source is unlikely for the Deccan basalts. The SiO_2-undersaturated primary magmas of the Deccan picrite and very high-Mg basalts are also distinctly

different from the SiO_2-saturated peridotite + MORB melts. Therefore, it can be concluded that all of the Deccan picrites and basalts under consideration originated from pristine lherzolite sources.

The NiO contents of the Fo_{90} olivine in equilibrium with the Deccan primary magmas, determined using the partition coefficient expression of Matzen et al. (2017) and the calculated mantle equilibration temperatures and MgO contents of the primary magmas and equilibrium olivines, are 0.32–0.55 wt% (one outlier at 0.13 wt%). These values are identical to the observed NiO contents of primitive olivines (Mg# 89, 0.30–0.52 wt% NiO) in basalts worldwide that erupted through a thick (> 70 km) lithosphere (Matzen et al. 2017). Matzen et al. (2017) also showed that the observed olivine compositions are consistent with melting of fertile peridotite. Thus, the calculated mantle equilibration temperatures and compositions of the Deccan primary magmas are reliable, and the primary magmas likely originated from a lherzolitic source.

Mantle melting conditions

Modeling shows that the primary magmas of the very high-Mg basalts and picrite from Saurashtra (MgO 11–14 wt%) were last equilibrated with the mantle at P–T conditions of 25–36 kbar/1452–1531 °C. These liquids originated from depths of ~ 83–117 km through melting of garnet lherzolite (Fig. 10). The primary magma of sample D44 shows equilibration just above the anhydrous peridotite solidus, indicating that it probably represents a very low-degree, near-fractional melt of the mantle. The equilibration P–T of this sample (36 kbar/1531 °C) constrains the mantle potential temperature to 1477–1495 °C, assuming adiabatic gradients of 1.0–1.5 °C/kbar.

The primary magmas of the high-Mg basalts (MgO 8.1–8.8 wt%) and low-Mg basalts were last equilibrated with spinel lherzolite at P–T conditions of 11.3–12.3 kbar/1310–1322 °C and 9.5–13.3 kbar/1289–1333 °C, respectively (Table 2). There is no significant difference in the P–T for the low-Mg mildly alkaline basalt (12.8 kbar/1322 °C) and tholeiitic basalts of Rajpipla-Navgam, indicating that mixed tholeiitic-alkalic magmas (Krishnamurthy et al. 2014) would also yield P–T of last equilibration with mantle in the same range. Similar P–T were also estimated for the primary magmas of tholeiites from Mumbai, and the Ambenali and Mahabaleshwar formations (8–13 kbar, 1268–1332 °C, Chatterjee and Sheth 2015). Thus, the primary magmas of most Deccan high-Mg and low-Mg tholeiites as well as the interlayered mildly alkaline basalts were last equilibrated with spinel lherzolite at similar P–T conditions. Considering that the average depth of Moho at the time of Deccan magmatism was ~ 40 km (~ 11 kbar, similar to present day, Rao et al.

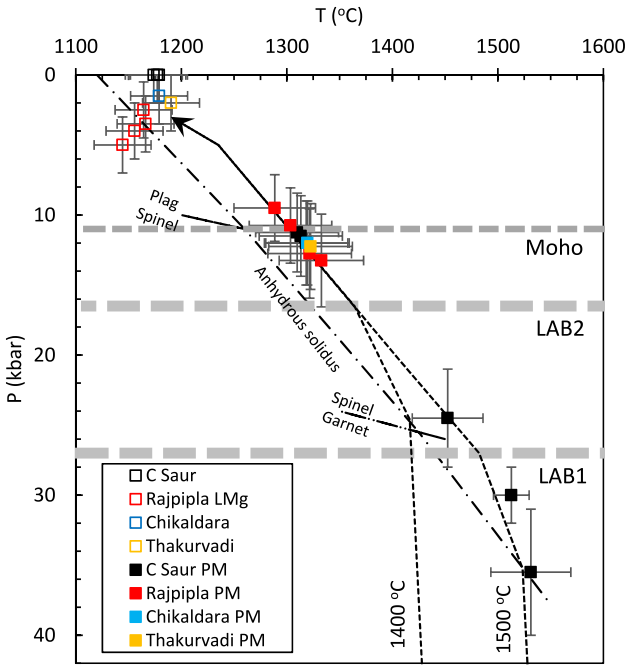

Fig. 10 Schematic diagram showing the P–T conditions of crystallization and last equilibration with mantle (primary magmas, PM) for selected Deccan low-Mg basalts, high-Mg basalts and picrite, the nominally anhydrous mantle solidus (Hirschmann 2000; Sarafian et al. 2017), approximate plagioclase-spinel (Till et al. 2012) and spinel-garnet (Grove et al. 2013) transition boundaries, possible crust-mantle (Moho) and lithosphere-asthenosphere (LAB1 and LAB2) boundaries, 1500 °C and 1400 °C adiabats and cooling paths (schematic) of the mantle melts that depend on the latent heat of melting, pooling characteristics, and pressure-dependent melt productivity (Behn and Grove 2015)

2015; Mohan and Ravi Kumar 2004), the pressure estimates indicate that the primary magmas of most Deccan tholeiites were last equilibrated with the mantle at or close to the Moho. Assuming adiabatic gradients of 1.0–1.5 °C/kbar, the apparent potential temperatures (T_P*, Krein et al. 2021) for the Deccan tholeiites with P–T of last equilibration with mantle of ~ 10–13 kbar/1290–1335 °C are ~ 1275–1325 °C. The apparent potential temperature reflects cooling of the mantle as it melts, and the true potential temperature can be calculated using the equation $T_P = T_P^* + F.L_H/C_P$, where F is the degree of melting, L_H is the latent heat of melting and C_P is the heat capacity (Krein et al. 2021).

The estimated equilibration temperatures of the primary magmas of the high-Mg and low-Mg basalts are consistently ~ 50 °C above the anhydrous peridotite solidus, indicating that they represent higher degree melts compared to sample D44 (Fig. 10). These primary magmas probably represent the average of spinel lherzolite melts that initially pooled at the base of a thinned lithosphere (LAB2). The average composition and P–T of pooled melts depend on the degree of melting and pooling characteristics (Behn

and Grove 2015; Krein et al. 2021). White and McKenzie (1995) estimated a maximum of ~ 15% melting for the Western Ghats basalts using rare earth element inversion and thermodynamic constraints. Sen (1995) also estimated a maximum of 15–18% melting for the Western Ghats basalts using major elements and batch and accumulated fractional melting models. On the other hand, Melluso et al. (2006) estimated only 5–11% maximum melting for the Gujarat high-Mg basalts based on major and incompatible trace elements and non-modal fractional melting models. However, the La_N/Sm_N and Dy_N/Yb_N ratios and a spinel lherzolite batch melting model suggest no difference in the degree of melting between the Western Ghats and the Gujarat tholeiites (Fig. 2e). For pooled melts, the mean degree of melting is approximately half of the maximum degree of melting (Langmuir et al. 1992). According to Krein et al.'s (2021) calculations, T_P* may be lower than T_P by ~ 120 °C for ~ 10% mean degree of melting and fully pooled melts. Hence, assuming ~ 15–18% maximum melting for the Deccan tholeiites, the true potential temperatures for the high-Mg and low-Mg basalts may be ~ 1400–1450 °C. Therefore, considering all samples, the estimated potential temperatures are in the range of ~ 1400–1500 °C. These temperatures are up to ~ 150 °C higher than the ambient mantle temperature of 1350 °C (present day value, Herzberg et al. 2010), and consistent with an origin of the Deccan tholeiites from a mantle plume.

Conclusions

Clinopyroxene-liquid and clinopyroxene composition thermobarometry indicates that all Deccan tholeiites including picrite, high-Mg basalt (MgO 8–12 wt%) and low-Mg basalt (42 samples from different areas) crystallized in the upper crust at maximum pressures of ~ 6 kbar and a temperature range of 1047–1221 °C. By contrast, the Deccan alkalic rocks (12 samples) crystallized at maximum pressures near the Moho (~ 12.7 kbar) and a broad range of temperatures (978–1289 °C).

Samples of high-Mg Deccan tholeiite that represent unmodified magmatic liquids are extremely rare. Reverse fractionation modeling indicates that the primary magmas of selected high-Mg basalts (5 samples) and a few low-Mg basalts (4 samples) that represent liquids were last equilibrated with the mantle at P–T conditions of 10–13 kbar and 1289–1333 °C. The primary magmas of very high-Mg basalts (MgO 11–12 wt%, 2 samples) and a picrite (1 sample) representing liquids that are even rarer, were last equilibrated with the mantle at P–T conditions of 25–36 kbar and 1452–1531 °C. Thus, the primary magmas of very high-Mg basalts and picrite were last equilibrated with garnet lherzolite, whereas the primary magmas of low-Mg and high-Mg basalts were last equilibrated with spinel lherzolite. The primary magma of a mildly alkaline basalt interlayered with low-Mg and high-Mg basalts was also last equilibrated with spinel lherzolite at similar conditions. The selected high-Mg basalts are 1–6% contaminated with the continental crust. Mantle potential temperatures based on the equilibration temperatures of the Deccan samples are 1400–1450 °C for the high-Mg and low-Mg basalts, and ~ 1500 °C for the picrite and the very high-Mg basalts. These results support derivation of the Deccan tholeiites from a mantle plume.

Supplementary Information The online version contains supplementary material available at https://doi.org/10.1007/s00410-024-02172-7.

Acknowledgements I am grateful to Hetu Sheth for providing the Chotila Hill samples for this study. I greatly appreciate the constructive and helpful comments of David Neave and an anonymous reviewer during peer review. These comments significantly improved the presentation of the manuscript.

Funding 'Open Access funding provided by the MIT Libraries'.

Data availability All data are published in the main article and the electronic supplement (Online Resource). The data are also available from the author upon request.

References

Ahmad I, Mondal MEA, Satyanarayanan M (2016) Geochemistry of Archean metasedimentary rocks of the Aravalli craton, NW India: Implications for provenance, paleoweathering and supercontinent reconstruction. J Asian Earth Sci 126:58–73

Andersen DJ, Lindsley DH (1988) Internally consistent solution models for Fe-Mg-Mn-Ti spinels: Fe-Ti oxides. Amer Mineral 73:714–726

Armstrong JT (1995) CITZAF—a package for correction programs for the quantitative electron microbeam x-ray analysis of thick polished materials, thin-films and particles. Microbeam Anal 4:177–200

Babechuk MG, Widdowson M, Kamber BS (2014) Quantifying chemical weathering intensity and trace element release from two contrasting basalt profiles, Deccan Traps, India. Chem Geol 363:56–75

Basu AR, Renne PR, Dasgupta DK, Teichmann F, Poreda RJ (1993) Early and late alkali igneous pulses and a high-^{3}He plume origin

for the Deccan flood basalts. Science 261:902–906. https://doi.org/10.1016/j.lithos.2020.105754

Basu AR, Saha-Yannopoulos A, Chakrabarty P (2020a) A precise geochemical volcano-stratigraphy of the Deccan traps. Lithos 376–377:105754. https://doi.org/10.1016/j.lithos.2020.105754

Basu AR, Chakrabarty P, Szymanowski D, Ibañez-Mejia M, Schoene B, Ghosh N, Bastian Georg R (2020b) Widespread silicic and alkaline magmatism synchronous with the Deccan Traps flood basalts. India Earth Planet Sci Lett 552:116616. https://doi.org/10.1016/j.epsl.2020.116616

Beane JE, Hooper PR (1988) A note on the picrite basalts from the Western Ghats, Deccan Traps, India. Mem Geol Soc India 10:117–133

Beane JE, Turner CA, Hooper PR, Subbarao KV, Walsh JN (1986) Stratigraphy, composition and form of the Deccan Basalts, Western Ghats, India. Bull Volcanol 48:61–83. https://doi.org/10.1007/bf01073513

Behn MD, Grove TL (2015) Melting systematics in mid-ocean ridge basalts: Application of a plagioclase-spinel melting model to global variations in major element chemistry and crustal thickness. J Geophys Res Solid Earth 120:4863–4886. https://doi.org/10.1002/2015JB011885

Bhattacharji S, Chatterjee N, Wampler JM, Nayak PN, Deshmukh SS (1996) Indian intraplate and continental margin rifting, lithospheric extension and mantle upwelling in Deccan flood basalt volcanism near K/T boundary: evidence from mafic dike swarms. J Geol 104:379–398

Bindeman IN, Davis AM, Drake MJ (1998) Ion microprobe study of plagioclase-basalt partition experiments at natural concentration levels of trace elements. Geochim Cosmochim Acta 62(7):1175–1193

Biswas SK (1987) Regional tectonic framework, structure and evolution of the western marginal basins of India. Tectonophys 135:307–327

Blundy J, Melekhova E, Ziberna L, Humphreys MCS, Cerantola V, Brooker RA, McCammon CA, Pichavant M, Ulmer P (2020) Effect of redox on Fe–Mg–Mn exchange between olivine and melt and an oxybarometer for basalts. Contrib Miner Pet 175:103

Bohrson WA, Spera FJ (2001) Energy-constrained open-system magmatic processes II: Application of energy-constrained assimilation-fractional crystallization (EC-AFC) model to magmatic systems. J Pet 42:1019–1041

Bondre NR, Hart WK, Sheth HC (2006) Geology and geochemistry of the Sangamner mafic dike swarm, western Deccan volcanic province, India: implications for regional stratigraphy. J Geol 114:155–170

Bose MK (1973) Petrology and geochemistry of the igneous complex of Mount Girnar, Gujarat, India. Contrib Miner Pet 39:247–296

Canil D, O'Neill HSC (1996) Distribution of ferric iron in some upper mantle assemblages. J Pet 37(3):609–635

Casshyap SM, Aslam M (1992) Deltaic and shoreline sedimentation in Saurashtra Basin, western India: An example of infilling in an Early Cretaceous failed rift. J Sed Pet 62(6):972–991

Chatterjee N (2021) Origin of the primitive, strongly SiO_2-undersaturated alkalic rocks from the Deccan Traps by low-degree mantle melting and high-pressure fractional crystallization. Contrib Miner Pet 176:31

Chatterjee N (2023) Origin of the Paleoproterozoic basaltic dikes from the central and eastern Dharwar Craton and sills and volcanics from the adjoining Cuddapah Basin, southern India. Contrib Miner Pet 178:28. https://doi.org/10.1007/s00410-023-02012-0

Chatterjee N, Bhattacharji S (2001) Origin of the felsic and basaltic dykes and flows in the Rajula-Palitana-Sihor area of the Deccan Traps, Saurashtra, India: a geochemical and geochronological study. Int Geol Rev 43:1094–1116

Chatterjee N, Ghose NC (2023) Thermobarometry of the Rajmahal Continental Flood Basalts and their primary magmas: Implications for the magmatic plumbing system. Minerals 13(3):426. https://doi.org/10.3390/min13030426

Chatterjee N, Sheth H (2015) Origin of the Powai ankaramite, and the composition, P-T conditions of equilibration and evolution of the primary magmas of the Deccan tholeiites. Contrib Miner Pet 169:32

Cohen TH, Sen G (1994) Fractionation and ascent of Deccan Trap magmas: An experimental study at 6 kilobar pressure. In: Subbarao KV (ed) Volcanism. Geol Soc India, pp 173–186

Courtillot V, Gallet Y, Rocchia R, Féraud G, Robin E, Hofmann C, Bhandari N, Ghevariya ZG (2000) Cosmic markers, $^{40}Ar/^{39}Ar$ dating and paleomagnetism of the KT sections in the Anjar area of the Deccan large igneous province. Earth Planet Sci Lett 182:137–156

Cox KG (1980) A model for flood basalt vulcanism. J Pet 21:629–650

Cox KG, Hawkesworth CJ (1984) Relative contribution of crust and mantle to flood basalt magmatism, Mahabaleshwar area, Deccan Traps. Phil Trans R Soc London A310:627–641

Cox KG, Hawkesworth CJ (1985) Geochemical stratigraphy of the Deccan Traps at Mahabaleshwar, Western Ghats, India, with implication for open system processes. J Pet 26:355–387

Cucciniello C, Demonterova EI, Sheth H, Pande K, Vijayan A (2015) $^{40}Ar/^{39}Ar$ geochronology and geochemistry of the Central Saurashtra mafic dyke swarm: insights into magmatic evolution, magma transport, and dyke-flow relationships in the northwestern Deccan Traps. Bull Volcanol 77:45. https://doi.org/10.1007/s00445-015-0932-0

Cucciniello C, Choudhary AK, Pande K, Sheth H (2019) Mineralogy, geochemistry and $^{40}Ar–^{39}Ar$ geochronology of the Barda and Alech complexes, Saurashtra, northwestern Deccan Traps: early silicic magmas derived by flood basalt fractionation. Geol Mag 156:1668–1690. https://doi.org/10.1017/S0016756818000924

Cucciniello C, Sheth H, Duraiswami RA, Wegner W, Koeberl C, Das T, Ghule V (2020) The Southeastern Saurashtra dyke swarm, Deccan Traps: Magmatic evolution of a tholeiitic basalt–basaltic andesite–andesite–rhyolite suite. Lithos 376–377:105759

De Wall HD, Regelous A, Schulz B, Hahn G, Bestmann M, Sharma KK (2021) Neoproterozoic geodynamics in NW India – evidence from Erinpura granites in the South Delhi Fold Belt. Int Geol Rev. https://doi.org/10.1080/00206814.2021.1907623

Dessai AG, Viegas A (2010) Petrogenesis of alkaline rocks from Murud-Janjira in the Deccan Traps, Western India. Mineral Pet 98:297–311

Dessai AG, Rock NMS, Griffin BJ, Gupta D (1990) Mineralogy and petrology of some xenolth bearing alkaline dykes associated with Deccan magmatism, south of Bombay, India. Eur J Min 2:667–685

Devey CW, Lightfoot PC (1986) Volcanological and tectonic control of stratigraphy and structure in the western Deccan Traps. Bull Volcanol 48:195–207

Dongre A, Viljoen KS, Rathod A (2018) Mineralogy and geochemistry of picro-dolerite dykes from the central Deccan Traps flood basaltic province, India, and their geodynamic significance. Mineral Pet 112:267–277. https://doi.org/10.1007/s00710-017-0539-6

Eddy MP, Schoene B, Samperton KM, Keller G, Adatte T, Khadri SF (2020) U-Pb zircon age constraints on the earliest eruptions of the Deccan Large Igneous Province, Malwa Plateau. India Earth Planet Sci Lett 540:116249

Fisk MR, Upton BGJ, Ford CE, White WM (1988) Geochemical and experimental study of the genesis of magmas of Reunion Island, Indian Ocean. J Geophys Res Solid Earth 93:4933–4950. https://doi.org/10.1029/jb093ib05p04933

Gao S, Takahashi E, Suzuki T (2017) High-Pressure melting experiments on basalt-peridotite layered source (KLB-1/N-MORB): Implications for magma genesis in Hawaii. Int J Geosci 8:1–15. https://doi.org/10.4236/ijg.2017.81001

Glišović P, Forte AM (2017) On the deep-mantle origin of the Deccan Traps. Science 355:613–616

Green DH, Falloon TJ, Eggins SM, Yaxley GM (2001) Primary magmas and mantle temperatures. Eur J Miner 13:437–451

Grove TL (1993) Corrections to expressions for calculating mineral components in "Origin of calc-alkaline series lavas at Medicine Lake volcano by fractionation, assimilation and mixing" and "Experimental petrology of normal MORB near the Kane Fracture Zone: 22°–25°N, mid-Atlantic ridge." Contrib Miner Pet 114:422–424

Grove TL, Gerlach DC, Sando TV (1982) Origin of calc-alkaline series lavas at Medicine lake volcano by fractionation, assimilation and mixing. Contrib Miner Pet 80:160–182

Grove TL, Holbig ES, Barr JA, Till CB, Krawczynski MJ (2013) Melts of garnet lherzolite: experiments, models and comparison to melts of pyroxenite and carbonated lherzolite. Contrib Miner Pet 166:887–910

Grove TL, Kinzler R, Bryan W (1992) Fractionation of mid-ocean ridge basalt (MORB). In: Phipps Morgan J, Blackman D, Sinton J (eds) Mantle flow and melt generation at mid-ocean ridges, geophysical monograph 71. AGU, Washington DC, pp 281–310

Hari KR, Chalapathi Rao NV, Swarnkar V, Hou G (2014) Alkali feldspar syenites with shoshonitic affinities from Chhotaudepur area: Implication for mantle metasomatism in the Deccan large igneous province. Geosci Front 5(2):261–276

Herzberg C, Asimow PD, Arndt N, Niu Y, Lesher CM, Fitton JG, Cheadle MJ, Saunders AD (2007) Temperatures in ambient mantle and plumes: constraints from basalts, picrites and komatiites. Geochem Geophys Geosyst 8:Q02006. https://doi.org/10.1029/2006GC001390

Herzberg C, Condie K, Korenaga J (2010) Thermal history of the Earth and its petrological expression. Earth Planet Sci Lett 292:79–88

Herzberg C, Vidito C, Starkey NA (2016) Nickel-cobalt contents of olivine record origins of mantle peridotite and related rocks. Am Miner 101:1952–1966

Higgins O, Sheldrake T, Caricchi L (2022) Machine learning thermobarometry and chemometry using amphibole and clinopyroxene: a window into the roots of an arc volcano (Mount Liamuiga, Saint Kitts). Contrib Miner Pet 177:10. https://doi.org/10.1007/s00410-021-01874-6

Hirschmann MM (2000) Mantle solidus: experimental constraints and the effects of peridotite composition. Geochem Geophys Geosyst 1:1042

Hirschmann MM, Kogiso T, Baker MB, Stolper EM (2003) Alkalic magmas generated by partial melting of garnet pyroxenite. Geology 31:481–484

Jayananda M, Chardon D, Peucat JJ, Capdevila R (2006) 2.61 Ga potassic granites and crustal reworking in the western Dharwar craton, south India: tectonic, geochronologic and geochemical constraints. Precamb Res 150:1–26

Jayananda M, Santosh M, Aadhiseshan KR (2018) Formation of Archean (3600–2500 Ma) continental crust in the Dharwar Craton, southern India. Earth-Sci Rev 181:12–42

Karmalkar NR, Griffin WL, O'Reilly S (2000) Ultramafic xenoliths from Kutch, Northwest India: plume-related mantle samples? Int Geol Rev 42(5):416–444

Karmalkar NR, Rege S, Griffin WL, O'Reilly SY (2005) Alkaline magmatism from Kachchh, NW India: implications for plume-lithosphere interactions. Lithos 81:101–119

Khanna TC, Kanakdande PP, Bizimis M, Arora K (2023) Geochemical benchmarks in the Phanerozoic LIPs constrained from well-cores in the Deccan Volcanic Province. India Lithos 462–463:107403. https://doi.org/10.1016/j.lithos.2023.107403

Kinzler RJ (1997) Melting of mantle peridotite at pressures approaching the spinel to garnet transition: application to mid-ocean ridge basalt petrogenesis. J Geophys Res 102:853–874

Kinzler R, Grove TL (1992a) Primary magmas of mid-ocean ridge basalts, 1. Exp Result Jour Geophys Res 97:6885–6906. https://doi.org/10.1029/91JB02840

Kinzler RJ, Grove TL (1992b) Primary magmas of mid-ocean ridge basalts 2. Appl Jour Geophys Res 97:6907–6926

Klein EM, Langmuir CH (1987) Global correlations of ocean ridge basalt chemistry with axial depth and crustal thickness. J Geophys Res 92:8089–8115

Kogiso T, Hirschmann MM, Pertermann M (2004) High-pressure partial melting of mafic lithologies in the mantle. J Petrol 45(12):2407–2422. https://doi.org/10.1093/petrology/egh057

Krein SB, Molitor ZJ, Grove TL (2021) ReversePetrogen: A Multiphase dry reverse fractional crystallization-mantle melting thermobarometer applied to 13,589 mid-ocean ridge basalt glasses. J Geophys Res Solid Earth 126:e2020JB021292

Krishnamurthy P, Cox KG (1977) Picrite basalts and related lavas from the Deccan Traps of Western India. Contrib Miner Pet 62:53–75

Krishnamurthy P, Pande K, Gopalan K, MacDougall JD (1999) Mineralogical and chemical studies on alkaline basaltic rocks of Kutch, Gujarat, India. Mem Geol Soc India 43:757–783

Krishnamurthy P, Gopalan K, Macdougall JD (2000) Olivine compositions in picrite basalts and the Deccan volcanic cycle. J Pet 41:1057–1069

Krishnamurthy P, Mahoney JJ, Gopalan K, MacDougall JD (2014) Clinopyroxene compositions in the Deccan and Rajmahal Traps and their bearing on magma types and evolution. J Asian Earth Sci 84:102–117. https://doi.org/10.1016/j.jseaes.2013.09.023

Langmuir CH, Klein EM, Plank T (1992) Petrological systematics of mid-ocean ridge basalts: Constraints on melt generation beneath ocean ridges. Mantle flow and melt generation at mid-ocean ridges. In: Morgan JP, Blackman DK, Sinton JM (eds) Mantle flow and melt generation at mid-ocean ridges, Geophysical Monograph Series 71. AGU, Washington DC, pp 183–280

Le Bas MJ (2000) IUGS reclassification of the high-Mg and picritic volcanic rocks. J Pet 41:1467–1470

Le Bas MJ, Le Maitre RW, Streckeisen A, Zanettin B (1986) A chemical classification of volcanic rocks based on the total alkali-silica diagram. J Pet 27:745–750

Lightfoot PC, Hawkesworth CJ, Devey CW, Rogers NW, van Calsteren PWC (1990) Source and differentiation of Deccan Trap lavas: implications of geochemical and mineral chemical variations. J Pet 31:1165–1200

MacDonald A, Ubide T, Mollo S, Pontesilli A, Masotta M (2023) The influence of undercooling and sector zoning on clinopyroxene-melt equilibrium and thermobarometry. J Pet 64(10):egad074. https://doi.org/10.1093/petrology/egad074

Macdonald GA, Katsura T (1964) Chemical composition of Hawaiian lavas. J Pet 5:82–133

Mahoney JJ, Macdougall JJ, Lugmair JD, Gopalan GW, Krishnamurthy K (1985) Origin of contemporaneous tholeiitic and K-rich alkalic lavas: a case study from the northern Deccan Plateau, India. Earth Planet Sci Lett 73:39–53

Matthews S, Wong K, Shorttle O, Edmonds M, Maclennan J (2021) Do olivine crystallization temperatures faithfully record mantle temperature variability? Geochem Geophys Geosys 22:e2020GC009157. https://doi.org/10.1029/2020GC009157

Matzen AK, Wood BJ, Baker MB, Stolper EM (2017) The roles of pyroxenite and peridotite in the mantle sources of oceanic basalts. Nat Geosci 10:530–535

McDonough WF, Sun S-S (1995) The composition of the Earth. Chem Geol 120(3–4):223–253

Melluso L, Sethna SF (2011) Mineral Compositions in the Deccan Igneous Rocks of India: An Overview. In: Ray J, Sen G, Ghosh B (eds) Topics in Igneous Petrology. Springer, Dordrecht, pp 135–159

Melluso L, Beccaluva L, Brotzu P, Gregnanin A, Gupta AK, Morbidelli L, Traversa G (1995) Constraints on the mantle sources of the Deccan Traps from the petrology and geochemistry of the basalts of Gujarat State (Western India). J Pet 36:1393–1432

Melluso L, Sethna SF, D'Antonio M, Javeri P, Bennio L (2002) Geochemistry and petrogenesis of soidic and potassic mafic alkaline rocks in the Deccan Volcanic Province, Mumbai area (India). Miner Pet 74:323–342

Melluso L, Mahoney JJ, Dallai L (2006) Mantle sources and crustal input as recorded in high-Mg Deccan Traps basalts of Gujarat (India). Lithos 89(3–4):259–274

Melluso L, de Gennaro R, Rocco I (2010) Compositional variations of chromiferous spinel in Mg-rich rocks of the Deccan Traps. India J Earth Syst Sci 119(3):343–363

Mitchell C, Widdowson M (1991) A geological map of the southern Deccan Traps, Indian and its structural implications. J Geol Soc Lond 148:495–505

Mohan G, Ravi Kumar M (2004) Seismological constraints on the structure and composition of western Deccan volcanic province from converted phases. Geophys Res Lett 31:L02601

Morimoto N, Fabries J, Ferguson AK, Ginzburg IV, Ross M, Seifert FA, Zussman L, Aoki K, Gottardi G (1988) Nomenclature of pyroxenes. Miner Mag 52:535–550

Naqvi SM, Condie KC, Allen P (1983) Geochemistry of some unusual Early Archaean sediments from Dharwar Craton, India. Precam Res 22:125–147

Neave DA, Putirka KD (2017) A new clinopyroxene-liquid barometer, and implications for magma storage pressures under Icelandic rift zones. Amer Mineral 102:777–794 http://www.minsocam.org/MSA/AmMin/special-collections.html

Nesbitt HW, Young GM (1982) Early Proterozoic climates and plate motions inferred from major element chemistry of lutites. Nature 299:715–717

Pande K, Cucciniello C, Sheth H, Vijayan A, Sharma KK, Purohit R, Jagadeesan KC, Shinde S (2017) Polychronous (early Cretaceous to Palaeogene) emplacement of the Mundwara alkalic complex, Rajasthan, India: $^{40}Ar/^{39}Ar$ geochronology, petrochemistry and geodynamics. Intern J Earth Sci 106:1487–1504

Peng ZX, Mahoney JJ (1995) Drillhole lavas in the Deccan Traps and the evolution of the Réunion plume. Earth Planet Sci Lett 134:169–185

Peng ZX, Mahoney J, Hooper P, Harris C, Beane J (1994) A role for lower continental crust in flood basalt genesis? Isotopic and incompatible element study of the lower six formations of the western Deccan Traps. Geochim Cosmochim Acta 58:267–288

Peng ZX, Mahoney JJ, Hooper PR, MacDougall JD, Krishnamurthy P (1998) Basalts of the northeastern Deccan Traps, India: isotopic and elemental geochemistry and relation to southwestern Deccan stratigraphy. J Geophys Res 103:29843–29865

Pertermann M, Hirschmann MM (2003) Anhydrous partial melting experiments on MORB-like eclogite: phase relations, phase compositions and mineral-melt partitioning of major elements at 2–3 GPa. J Pet 44:2173–2201. https://doi.org/10.1093/petrology/egg074

Pilet S, Baker MB, Stolper EM (2008) Metasomatized lithosphere and the origin of alkaline lavas. Science 320:916–919

Presnall DC, Gudfinnsson GH, Walter MJ (2002) Generation of mid-ocean ridge basalts at pressures from 1 to 7 GPa. Geochim Cosmochim Acta 66:2073–2090

Putirka KD (2008) Thermometers and barometers for volcanic systems. Rev Miner Geochem 69:61–120

Putirka KD, Perfit M, Ryerson FJ, Jackson MG (2007) Ambient and excess mantle temperatures, olivine thermometry, and active vs. passive upwelling. Chem Geol 241:177–206

Rao KM, Ravi Kumar M, Rastogi BK (2015) Crust beneath the northwestern Deccan Volcanic Province, India: Evidence for uplift and magmatic underplating. J Geophys Res Solid Earth 120:3385–3405

Roeder PL, Emslie RF (1970) Olivine liquid equilibrium. Contrib Miner Pet 29:275–289

Rushmer T (1991) Partial melting of two amphibolites: contrasting experimental results under fluid-absent conditions. Contrib Miner Pet 107:41–59

Sarafian E, Gaetani GA, Hauri EH, Sarafian AR (2017) Experimental constraints on the damp peridotite solidus and oceanic mantle potential temperature. Science 355(6328):942–945

Schoene B, Eddy MP, Samperton KM, Keller CB, Keller G, Adatte T, Khadri SFR (2019) U-Pb constraints on pulsed eruption of the Deccan Traps across the end-Cretaceous mass extinction. Science 363:862–866

Sen G (1988) Possible depth of origin of primary Deccan tholeiite magma. Mem Geol Soc India 10:34–51

Sen G (1995) A simple petrologic model for the generation of Deccan Trap magmas. Int Geol Rev 37:825–850

Sheth HC, Melluso L (2008) The Mount Pavagadh volcanic suite, Deccan Traps: geochemical stratigraphy and magmatic evolution. J Asian Earth Sci 32:5–21

Sheth HC, Choudhary AK, Bhattacharyya S, Cucciniello C, Laishram R, Gurav T (2011) The Chogat-Chamardi subvolcanic complex, Saurashtra, northwestern Deccan Traps: geology, petrochemistry, and petrogenetic evolution. J Asian Earth Sci 41:307–324

Sheth HC, Choudhary AK, Cucciniello C, Bhattacharyya S, Laishram R, Gurav T (2012) Geology, petrochemistry, and genesis of the bimodal lavas of Osham Hill, Saurashtra, northwestern Deccan Traps. J Asian Earth Sci 43:176–192

Sheth HC, Zellmer GF, Kshirsagar PV, Cucciniello C (2013) Geochemistry of the Palitana flood basalt sequence and the Eastern Saurashtra dykes, Deccan Traps: clues to petrogenesis, dyke-flow relationships, and regional lava stratigraphy. Bull Volcanol 75:701. https://doi.org/10.1007/s00445-013-0701

Sheth H, Pande K, Vijayan A, Sharma KK, Cucciniello C (2017) Recurrent early cretaceous, indo-madagascar (89–86 Ma) and deccan (66 Ma) alkalic magmatism in the Sarnu-Dandali complex, Rajasthan: 40Ar/39Ar age evidence and geodynamic significance. Lithos 284–285:512–524

Sheth H, Duraiswami R, Ghule V, Naik A, Das T (2022) Flood basalt structures and textures as guides to cooling histories and palaeoclimates: The Deccan Traps of Saurashtra, western India. Geol Mag 159(8):1415–1436. https://doi.org/10.1017/S0016756822000279

Sheth HC, Zellmer GF, Demonterova EI, Ivanov AV, Kumar R, Patel RK (2014) The deccan tholeiite lavas and dykes of ghatkoparpowai area, Mumbai, panvel flexure zone: geochemistry, stratigraphic status, and tectonic significance. J Asian Earth Sci 84:69–82

Simonetti A, Goldstein SL, Schmidberger SS, Viladkar SG (1998) Geochemical and Nd, Pb, and Sr isotope data from Deccan alkalic complexes: inferences for mantle sources and plume-lithosphere interaction. J Pet 39:1847–1864

Spera FJ, Bohrson WA (2001) Energy-constrained open-system magmatic processes I: general model and energy-constrained

assimilation and fractional crystallization (EC-AFC) formulation. J Pet 42:999–1018. https://doi.org/10.1093/petrology/42.5.999

Sprain CJ, Renne PR, Vanderkluysen L, Pande K, Self S, Mittal T (2019) The eruptive tempo of Deccan volcanism in relation to the Cretaceous-Paleogene boundary. Science 363:866–870

Subbarao KV, Bodas MS, Hooper PR, Walsh JN (1988) Petrogenesis of Jawhar and Igatpuri formations, western Deccan basalt province, India. Mem Geol Soc India 10:253–280

Sun S-S, McDonough WF (1989) Chemical and isotopic systematics of oceanic basalts: implications for mantle compostion and processes. In: Saunders AD, Norry DJ (eds) Magmatisms in the ocean basins. Geol Soc London, London, Spec Publ 42:313–345

Till CB (2017) A review and update of mantle thermobarometry for primitive arc magmas. Amer Miner 102:931–947

Till CB, Grove TL, Krawczynski MJ (2012) A melting model for variably depleted and enriched lherzolite in the plagioclase and spinel stability fields. J Geophys Res 117:B06206. https://doi.org/10.1029/2011JB009044

Till CB, Grove TL, Carlson RW, Fouch MJ, Donnelly-Nolan JM, Wagner LS, Hart WK (2013) Depths and temperatures of <10.5 Ma mantle melting and the lithosphere-asthenosphere boundary below southern Oregon and northern California. Geochem Geophys Geosyst 14:864–879. https://doi.org/10.1002/ggge.20070

Tormey DR, Grove TL, Bryan WB (1987) Experimental petrology of normal MORB near the Kane Fracture Zone: 22–25°N, mid-Atlantic Ridge. Contrib Miner Pet 96:121–139

Ubide T, Mollo S, Zhao J, Nazzari M, Scarlato P (2019) Sector-zoned clinopyroxene as a recorder of magma history, eruption triggers, and ascent rates. Geochim Cosmochim Acta 251:265–283. https://doi.org/10.1016/j.gca.2019.02.021

Vanderkluysen L, Mahoney JJ, Hooper PR, Sheth HC, Ray R (2011) The feeder system of the Deccan Traps (India): Insights from dyke geochemistry. J Pet 52:315–343. https://doi.org/10.1093/petrology/egq082

Vijayan A, Sheth H, Sharma KK (2016) Tectonic significance of dykes in the Sarnu-Dandali alkalic complex, Rajasthan, northwestern Deccan Traps. Geosci Front 7:783–791

Villiger S, Ulmer P, Muntener O, Thompson AB (2004) The liquid line of descent of anhydrous, mantle-derived, tholeiitic liquids by fractional and equilibrium crystallization—an experimental study at 10 GPa. J Pet 45(12):2369–2388

Wadia DN (1975) Geology of India, 4th edn. Tata McGraw-Hill, New Delhi, p 508

White RS, McKenzie D (1995) Mantle plumes and flood basalts. J Geophys Res 100:17543–17585

Yang HJ, Kinzler RJ, Grove TL (1996) Experiments and models of anhydrous, basaltic olivine-plagioclase-augite saturated melts from 0.001 to 10 kbar. Contrib Miner Pet 124:1–18